Gallium Passive Decay Heat Removal Systems Design and Evaluation for IVR-ERVCS of APR 1400 and PDHRS of UCFR-100

Sarah Kang

Department of Mechanical & Nuclear Engineering

Graduate school of UNIST

Gallium Passive Decay Heat Removal Systems Design and Evaluation for IVR-ERVCS of APR 1400 and PDHRS of UCFR-100

A dissertation
submitted to the Graduate School of UNIST
in partial fulfillment of the
requirements for the degree of
Doctor of Philosophy of Science

Sarah Kang

06.19.2015
Approved by

Advisor
Prof. In Cheol Bang

Gallium Passive Decay Heat Removal Systems Design and Evaluation for IVR-ERVCS of APR 1400 and PDHRS of UCFR-100

Sarah Kang

This certifies that the dissertation of Sarah Kang is approved.

06.19.2015

Signature

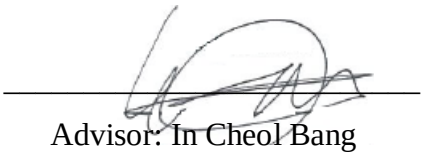

Advisor: In Cheol Bang

Signature

Jae Young Lee

Signature

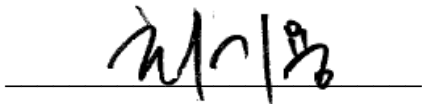

Ki-Yong Choi

Signature

Ji Hyun Kim

Signature

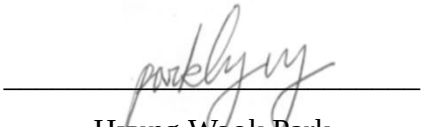

Hyung Wook Park

Abstract

The passive decay heat removal system is one of the important concepts of nuclear power plants. Because the principle of the system is based on laws of physics such as gravity or natural convection, it is able to function without electric power or actuation by control equipments. In this paper, the liquid metal, gallium-cooled passive decay heat removal systems of pressurized water reactor (PWR), APR 1400 and Ultra-long-life-Core fast Reactor, UCFR-100 were suggested and simulated using MARS-Ga code. The experimental study to investigate the natural convective heat transfer was also conducted.

Although MARS-LMR code was originally intended for a safety analysis of liquid metal-cooled fast reactor such as a sodium-cooled fast reactor, gallium properties were newly added to this code as so-called MARS-Ga code which is applicable for gallium cooled systems. The implementation of the properties for liquid metals in MARS-LMR code used the soft-sphere model based on Monte Carlo calculations for particles interacting with pair potentials, and the transport properties such as surface tension, thermal conductivity, and dynamic viscosity for the liquid and vapor state were also included.

In the experimental analysis, the natural convection heat transfer of liquid gallium was investigated in the rectangular loop which consists of an indirect heating block test section, a condenser, and the 1/2 inch SS 316L tubes as well as the orifice for measuring mass flowrate. The average Nusselt number of liquid gallium was measured within the heat flux range of 6.17×10^3 – 5.07×10^4 W/m^2. The mass flow rate for the natural convection of liquid gallium depending on power level was also compared by using CFD and MARS-Ga code.

In the numerical analyses, the evaluations of the gallium-water in-vessel corium retention through external reactor vessel cooling system (IVR-ERVCS) in APR 1400 and gallium-cooled passive decay heat removal system (PDHRS) in UCFR-100 were performed using MARS-Ga code. The attractive properties such as the low melting point, the high boiling point, and no reaction with water ensure that gallium can play an important role in nuclear safety as an alternative coolant in PWRs and SFRs.

In the gallium-water IVR-ERVCS, the generated decay heat is transferred to liquid gallium through the reactor pressure vessel and then removed from the water pool as a heat sink. The numerical analysis results showed that the temperature range of the liquid gallium is much lower than its boiling point and confirm the natural convection under a medium break loss of coolant accident (MBLOCA) and large break loss of coolant accident (LBLOCA). Because liquid gallium in this system didn't have a phase change, unlike water, the gallium-water IVR-ERVCS can provide stable and reliable cooling capability. Sensitivity studies were also performed by changing several parameters such as the initial temperature of liquid gallium and water pool inventory, and their results indicated that the working time of the gallium-water IVR-ERVCS depends on the inventory of the water pool using MARS-Ga code.

UCFR-100 is a 260MW_{th} / 100MW_e sodium-cooled fast reactor which requires no on-site refueling. UCFR-100 is a pool type reactor including the metallic fuels, intermediate heat exchangers, steam generators, and gallium-cooled PDHRS unlike the existing designs of sodium fast reactors. The safety analysis was performed for loss of flow (LOF) due to the pumping failure of primary pumps using MARS-Ga code. As a result, it confirmed that the liquid gallium can work properly as a boundary material between sodium and atmosphere for steady state and transient situation in UCFR-100.

Contents

List of figures

List of table

Nomenclature

C_n	fcc Madelung constant
C_p	constant-pressure specific heat [J/kg·K]
C_R	heat transfer coefficient [W/m^2·K]
C_v	constant-volume specific heat [J/kg·K]
D	diameter [m]
E_{coh}	cohesive energy [J/kg]
Gr	Grashof number
Gr_m	modified Grashof number, $\frac{D^3\rho^2\beta gqH}{\mu^3 AC_p}$
g	gravity [m/s^2]
H	height [m]
h	enthalpy [J/kg]
h	heat transfer coefficient [W/m^2·K]
K	boltzman constant
k	thermal conductivity [W/m·K]
L	characteristic length, length [m]
N	atomic weight [kg/mol]
N_G	geometric parameter
Nu_D	Nusselt number for cylinder (tube), $\frac{hD}{k}$
Nu_L	Nusselt number for common immersed (external flow) geometries, $\frac{hL}{k}$
Nu_m	Nusselt number (mean value)
$\dot{\mathbf{m}}$	mass flow rate [kg/s]
n	parameter
P	pressure [Pa]
Pr	Prandtl number
Q	multiplier
q	total heat [W]
R	flow resistance parameter

Ra_D Rayleigh number for cylinder (tube), $\frac{g\beta\left(T_{surface}-T_{fluid}\right)D^3}{\nu\alpha}$

Ra_L Rayleigh number for common immersed (external flow) geometries, $\frac{g\beta\left(T_{surface}-T_{fluid}\right)L^3}{\nu\alpha}$

Re Reynolds number

s entropy [J/kg]

T temperature [K]

u internal energy [J/kg]

v specific volume [m^3/kg]

Greek symbols

β thermal expansion coefficient [K^{-1}]

κ isothermal compressibility [Pa^{-1}]

ρ density [kg/m^3]

λ de Broglie wavelength [m]

ε parameter [J/atom]

σ parameter [m^3/atom]

σ surface tension [N/m]

μ viscosity [kg/m·s]

Subscripts

B buoyancy

b bubble

e electrical

eff effective

in inlet

m modified

out outlet

p pressure

ss	steady state
t	total
th	thermal
v	volume
0	reference

Chapter 1. Introduction

1.1 Background

This study proposes the use of liquid metal, gallium as a coolant in a decay heat removal system for the method to improve the nuclear safety. Gallium is the metal which can be liquid state near the room temperature. Because having the wide range of liquid phase and low oxygen reactivity and so on, gallium has difficult to phase change of explosion with water or atmosphere as shown in table 1-1[1-6]. In this study, it suggests that gallium can be a coolant in the external reactor vessel cooling system of pressurized water reactor, APR 1400 and the passive decay heat exchanger of ultra-long-life-core fast reactor, UCFR-100 respectively.

To evaluate the new safety systems using liquid gallium, the safety analysis code, MARS-LMR was selected. The MARS (Multi-dimensional analysis of reactor safety) code was developed by KAERI (Korea atomic energy research institute) for a multi-dimensional and multi-purpose realistic thermal-hydraulic system analysis of light water reactors. Although MARS code was originally intended for a safety analysis of light water reactors, several liquid metal properties such as sodium, lead bismuth eutectic (LBE) and so on were newly added to this code as so-called MARS-LMR. The properties of gallium were also added to this code as so-called MARS-Ga due to the need for performing predictive calculations relevant to gallium-cooled passive decay heat removal systems.

1.2 Research objectives and scope

The first part of this study introduced and performed the implementation of the implementation of the thermodynamic property file for liquid gallium and simultaneously, the natural convection experiment of liquid gallium in a rectangular loop was conducted in the second part. The third and fourth part consisted of the evaluation of the gallium-water IVR-ERVCS (In-vessel corium retention through external reactor vessel cooling system) and gallium-cooled PDHRS (Passive decay heat removal system) in nuclear power plants respectively.

Therefore, the objectives of this study are the generation of gallium property file using the theory in MARS-LMR to derive the fluid properties and validation of the gallium properties compared to the experimental data and evaluation of the gallium-cooled passive decay heat removal systems in APR 1400 and UCFR-100 using MARS-Ga.

Table 1-1. Comparison of thermo physical properties of liquid metals

	Ga	Na	Pb	LBE
Atomic weight	69.72	22.99	207.21	208
Melting point [K]	303	371	601	397
Boiling point [K]	2477	1165	2010	1943
Density [kg/m^3]	6084	925	10670	10300
Specific heat [J/kg·K]	397.9	1382	147.3	146
Thermal conductivity [W/m·K]	28.9	84.9	15.8	11
Viscosity [10^{-3}kg/m·s]	1.39	0.68	2.55	1.7

The properties of gallium were evaluated at 303K.

The properties of sodium, lead and LBE were evaluated at 373K, 603K and 573K respectively.

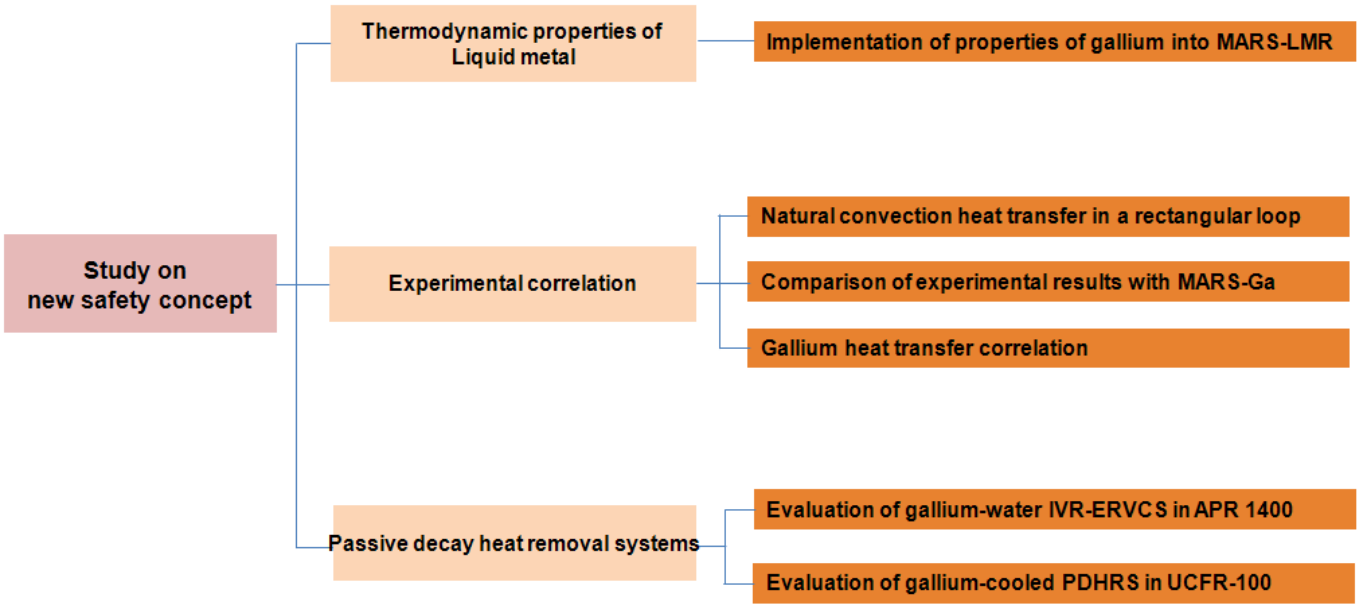

Fig. 1-1. Research scope

Chapter 2. Implementation of thermodynamic properties into MARS-LMR for liquid gallium

2.1 Introduction

In this study, the safety analysis code, MARS-LMR was selected. To simulate systems with the certain working fluids in the code, it needs the thermodynamic properties with information of the working fluids from the fluid property tables stored in thermodynamic property file (tpf). For example, tpfh2o and tpfna mean the property file of water and sodium respectively. In this part, the gallium properties are newly added to this code as so-called MARS-Ga due to the need for performing predictive calculations relevant to gallium-cooled passive decay heat removal systems. These fluid property tables are generated by computer program that calculate thermodynamic properties from formulations developed for each specific fluid[7]. The generated programs for liquid gallium are named stgga as does MARS-LMR. The fluid properties in the file include specific volume (v), internal energy (u), thermal expansion coefficient (β), isothermal compressibility (κ), specific heat (C_p), and entropy (s) at combinations of temperature and pressure. Transport properties such as surface tension, thermal conductivity, and dynamic viscosity are also needed.

2.2 Literature survey

In 1977, Young[8] published an equation of state (EOS) of several liquid metals including gallium based on the soft-sphere model. Enthalpy, volume, and sound speed were computed as functions of temperature and compared with experimental data. Based on the this paper, Blink[9] summarized Young's development of the EOS and demonstrate a computer program that plots isotherms, isentropes and constant energy lines on a P-V diagram of lithium. Tolli[7] also calculated the properties for helium, nitrogen, lithium, lithium-lead by the ATHENA/MOD1 computer program using the EOS of Young for fusion safety research. The properties of molten salts were also generated from the EOS that utilized a soft-sphere model[10]. KAERI also developed the properties of sodium and lead bismuth using same method[11].

2.3 Property formulations for liquid gallium

To generate the gallium property table by computer program, stgga, it needs the parameters of Helmholtz free energy equation as shown in eq. (2.1).

$$A = NKT\left[-\ln\frac{Ve}{N\lambda^3} + C_n\rho^{n/3}\left(\frac{\varepsilon}{kT}\right) + \frac{1}{2}(n+4)Q\rho^{n/9}\left(\frac{\varepsilon}{kT}\right)^{1/3} - \rho^m\left(\frac{\varepsilon}{kT}\right)\right] + E_{coh} \qquad (2.1)$$

In the brackets, the first term presents the kinetic energy, the second term is the static lattice potential energy, the third term is the thermal lattice potential energy correction, and the fourth term is the attractive potential energy[9]. In the second term ρ is the normalized density, $N\sigma^3/\sqrt{2V}$.

The pressure, energy, and entropy may be found from the general equation of Helmholtz free energy as shown in eq. (2.2).

$$A \equiv u - Ts \tag{2.2}$$

The change of the internal energy is as shown in eq. (2.3) and eq. (2.4) is obtained by replacing the form of internal energy using eq. (2.3).

$$du = Tds - pdv \tag{2.3}$$

$$dA = -pdv - sdT \tag{2.4}$$

Eq. (2-4) can be changed as shown in eq. (2.5).

$$dA = \left(\frac{\partial A}{\partial v}\right)dv + \left(\frac{\partial A}{\partial T}\right)dT \tag{2.5}$$

Therefore, the pressure, energy, and entropy can be obtained as follows.

$$P = -\left(\frac{\partial A}{\partial V}\right)_T \tag{2.6}$$

$$s = -\left(\frac{\partial A}{\partial T}\right)_V \tag{2.7}$$

$$u = A - T\left(\frac{\partial A}{\partial T}\right)_V \tag{2.8}$$

The specific heat is defined as the energy required raising the temperature of unit mass of a substance by one degree. An expression for the specific heat at constant pressure C_p can be obtained by considering a constant-pressure expansion or compression process[12]. It yields

$$C_p \equiv \left(\frac{\partial q}{\partial T}\right)_p \equiv \left(\frac{\partial h}{\partial T}\right)_p \tag{2.9}$$

The specific heat can easily be determined by using the definition of enthalpy :

$$C_p = \left(\frac{\partial u}{\partial T}\right)_p + p\left(\frac{\partial v}{\partial T}\right)_p \tag{2.10}$$

The volumetric thermal expansion, β and the isothermal compressibility, κ are defined using the relation of the specific heat by changing the term of the internal energy and entropy in eq. (2.3) using eq. (2.11) and (2.12).

$$ds = \left(\frac{\partial s}{\partial T}\right)_v dT + \left(\frac{\partial s}{\partial v}\right)_T dv \tag{2.11}$$

$$du = \left(\frac{\partial u}{\partial T}\right)_v dT + \left(\frac{\partial u}{\partial v}\right)_T dv = C_v dT + \left(\frac{\partial u}{\partial v}\right)_T dv \tag{2.12}$$

Eq. (2.3) is changed as shown in eq. (2.13).

$$C_v dT + \left(\frac{\partial u}{\partial v}\right)_T dv = T\left(\frac{\partial s}{\partial T}\right)_v dT + \left[\left(\frac{\partial s}{\partial v}\right)_T - P\right] dv \tag{2.13}$$

Therefore,

$$C_v = T\left(\frac{\partial s}{\partial T}\right)_v \tag{2.14}$$

Using the constant-volume specific heat and Maxwell relations as shown in eq. (2.14) and (2.15), the change of the entropy, eq. (2.11) can be obtained as shown in eq. (2.16).

$$\left(\frac{\partial s}{\partial v}\right)_T = \left(\frac{\partial p}{\partial T}\right)_v \tag{2.15}$$

$$ds = \frac{C_v}{T} dT + \left(\frac{\partial p}{\partial T} \right)_v dv \tag{2.16}$$

The pressure-constant specific heat can be obtained using same method as shown in eq. (2.17).

$$ds = \frac{C_p}{T} dT + \left(\frac{\partial v}{\partial p} \right)_p dp \tag{2.17}$$

It starts the development of such the relation by equation the two ds relations as shown in eq. (2.16) and (2.17) and solving for dT.

$$dT = \frac{T\left(\frac{\partial p}{\partial T} \right)_v}{\left(C_p - C_v \right)} dv + \frac{T\left(\frac{\partial v}{\partial T} \right)_p}{\left(C_p - C_v \right)} dp \tag{2.18}$$

Choosing eq. (2.19) and differentiating, eq. (2.20) can be obtained.

$$dT = \left(\frac{\partial T}{\partial v} \right)_p dv + \left(\frac{\partial T}{\partial p} \right)_v dp \tag{2.19}$$

$$C_p - C_v = T\left(\frac{\partial v}{\partial T} \right)_p \left(\frac{\partial p}{\partial v} \right)_v \tag{2.20}$$

The alternative form of this relation is obtained by using the cyclic relation as shown in eq. (2.21) and (2.22).

$$\left(\frac{\partial p}{\partial T} \right)_v \left(\frac{\partial T}{\partial v} \right)_p \left(\frac{\partial v}{\partial p} \right)_T = -1 \tag{2.21}$$

$$\left(\frac{\partial p}{\partial T} \right)_v = -\left(\frac{\partial v}{\partial T} \right)_p \left(\frac{\partial p}{\partial v} \right)_T \tag{2.22}$$

Substituting the result into eq. (2.20), eq. (2.23) can be obtained.

$$C_p - C_v = -T\left(\frac{\partial v}{\partial T}\right)_p^2 \left(\frac{\partial p}{\partial v}\right)_v \tag{2.23}$$

This relation can be expressed in terms of two other thermodynamic properties called the volumetric thermal expansion, β and the isothermal compressibility, κ which are defined as shown in eq. (2.24) and (2.25).

$$\beta = \frac{1}{v}\left(\frac{\partial v}{\partial T}\right)_p \tag{2.24}$$

$$\kappa = -\frac{1}{v}\left(\frac{\partial v}{\partial p}\right)_T \tag{2.25}$$

To solve above equations, it needs parameters such as n, m, Q, C_n, ε, σ for gallium as shown in table 2-1. ε, σ could be gained by solving the pressure and energy equation like eq. (2.6) and (2.8) and other parameters were obtained from the paper of Young[8]. The generated properties by computer program are as shown in eq. (2.6) – (2.25).

The saturation equation and transport properties are also as follows[4,13-14].

$$\log P = 101325 \times 10^{\left(\frac{-14900}{T+200} - 0.515\log(T+200) + 7.34\right)} \tag{2.26}$$

$$\sigma = 708 - 3.9 \times 10^5 \left(T - 303\right) \tag{2.27}$$

$$\mu = 0.01207 - 5.754 \times 10^{-5} T + 7.891 \times 10^{-8} T^2 \tag{2.28}$$

$$k = 7.08 + 8.014 \times 10^{-2} T - 2.7 \times 10^5 T^2 \tag{2.29}$$

2.4 Result and discussion

The thermodynamic properties of gallium can be obtained using computer program, stgga. At first, the code version and liquid name were printed and then day and time were printed. Using the input text file, "stggai.i" having the series of the temperature and pressure to use as the standard of the properties of gallium, this computer program checked the number and ascending order of temperature and pressure respectively. Before the calculating the properties, this computer program also displayed the data limit such as triple and critical point and calculated the number of words in the binary table. The calculating table consist of the three part, table 3,4,5. Table 3 stored saturation properties of gallium at liquid and vapor state (temperature vs. pressure). Table 4 also stored saturation properties of gallium at liquid and vapor state (pressure vs. temperature). Finally, table 5 stored the thermodynamic properties of gallium according to the entire range of temperature having each pressure respectively.

Fig. 2-1 shows the comparison of the saturation equation of gallium and the line in this figure indicates eq. (2.26) based on Cochran and Foster[13]. It confirmed that the each point shows good agreement.

Using the information of gallium in part 2.3, the data of thermodynamic properties can be obtained like specific volume, internal energy, thermal expansion, isothermal compressibility, specific heat, and entropy for each combination of the temperature and pressure. Fig. 2-2 ~ 2-4 show the comparisons of generated thermodynamic table data with existing correlations for gallium and they show good agreements.

By using this thermodynamic property table file, tpfga, the thermal hydraulic systems of liquid gallium can be simulated for numerical and parametric studies.

Table 2-1. Thermo physical properties of gallium

		Value
Cohesive energy [J/kg]		3.9×10^{6}
Critical point	Temperature [K]	7200
	Pressure [Pa]	4.0×10^{8}
	Specific volume [m^3/kg]	5.682×10^{-4}
Triple point	Temperature [K]	302
	Pressure [Pa]	2.975×10^{-19}
	Specific volume [m^3/kg]	1.639×10^{-4}
Parameters	n	8.8
	m	0.75
	Q	0.95
	ε	1.42×10^{-18}
	σ	3.1×10^{-30}
	C_n	11.9

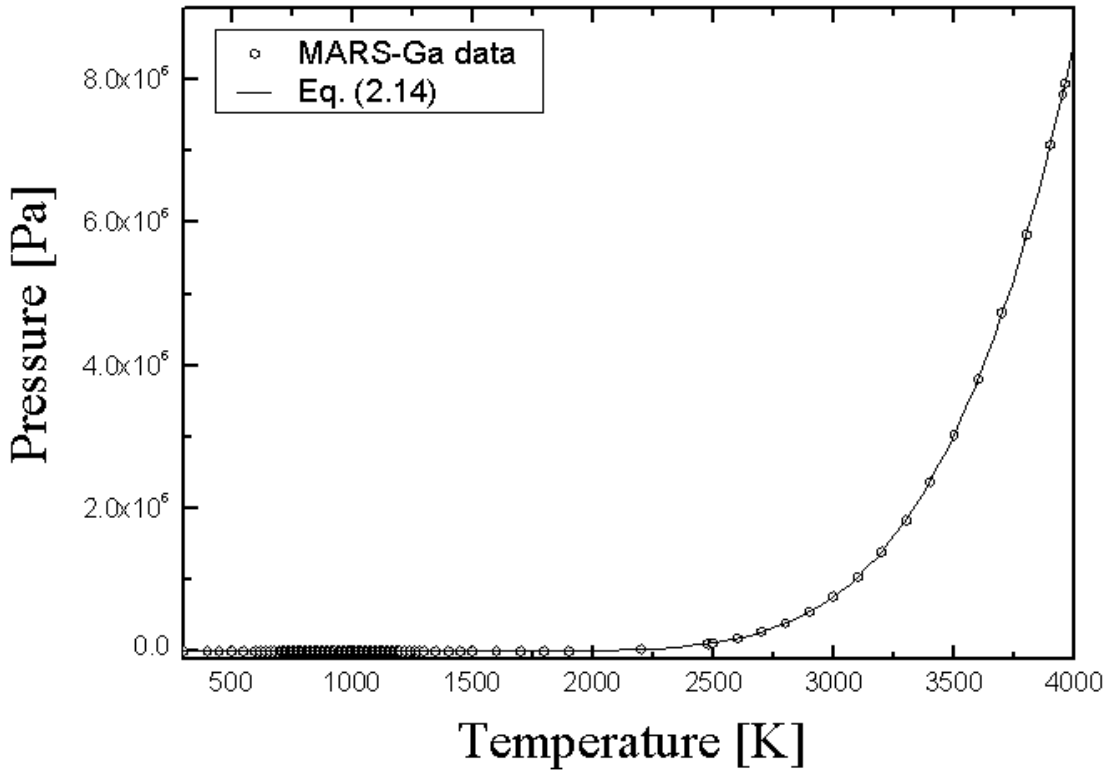

Fig. 2-1 Saturation equation of gallium

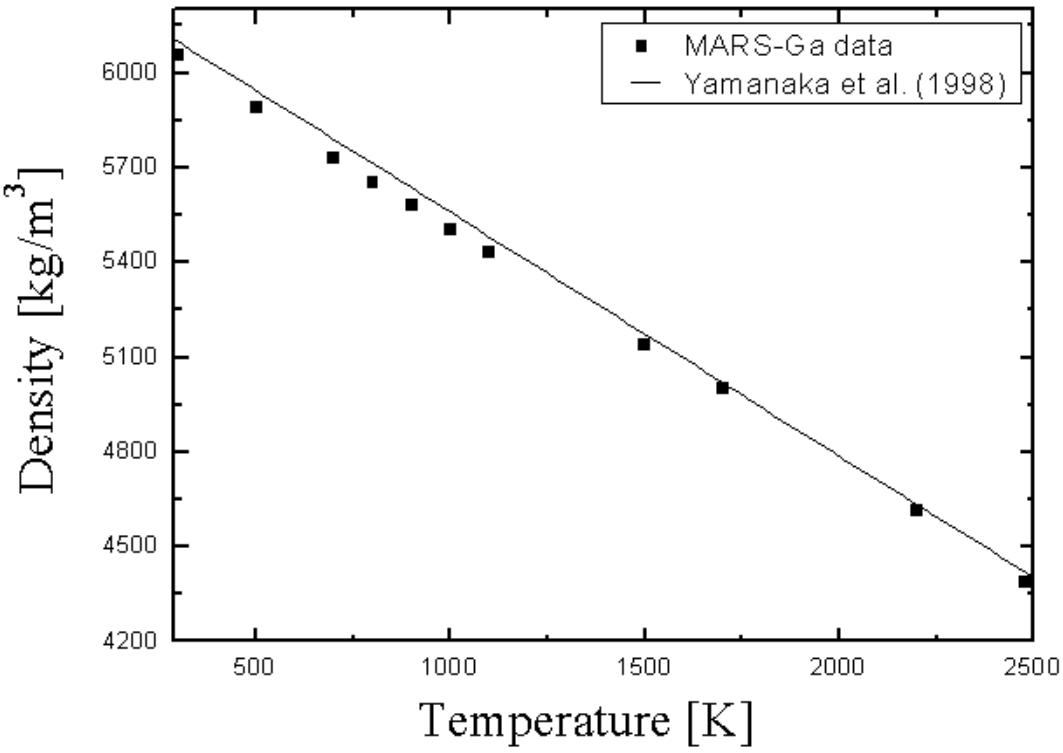

Fig. 2-2 Density comparison of generated thermodynamic table data with Yamanaka et al. for gallium

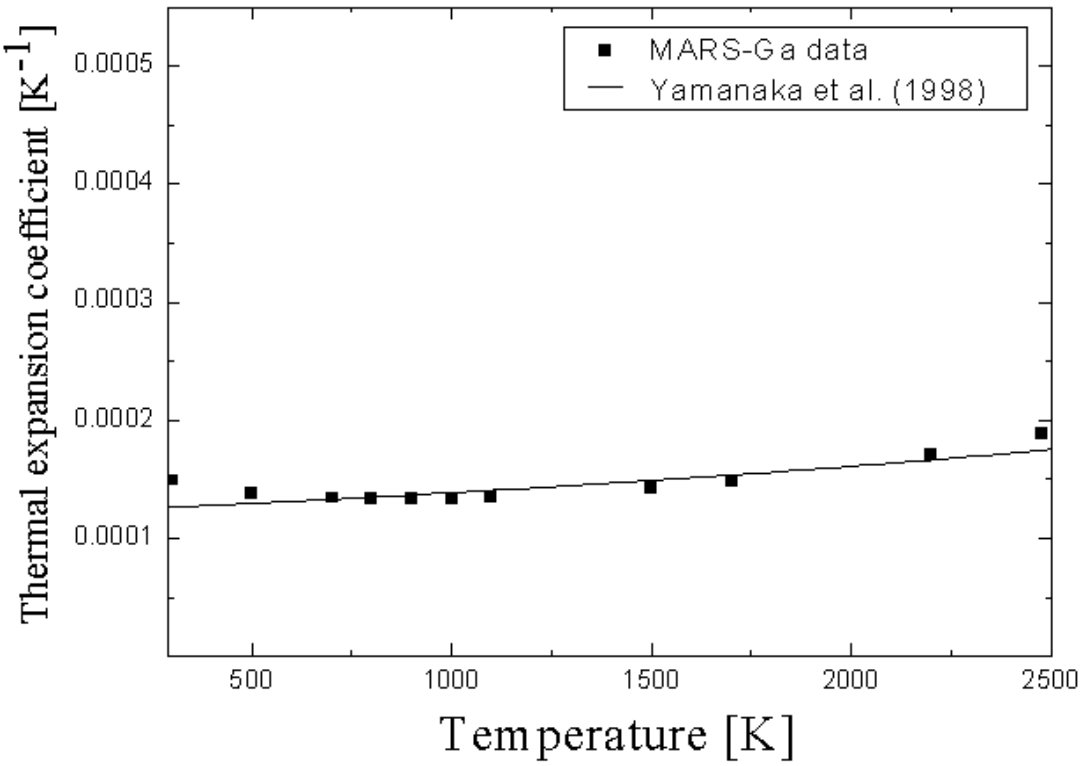

Fig. 2-3 Thermal expansion comparison of generated thermodynamic table data with Yamanaka et al. for gallium

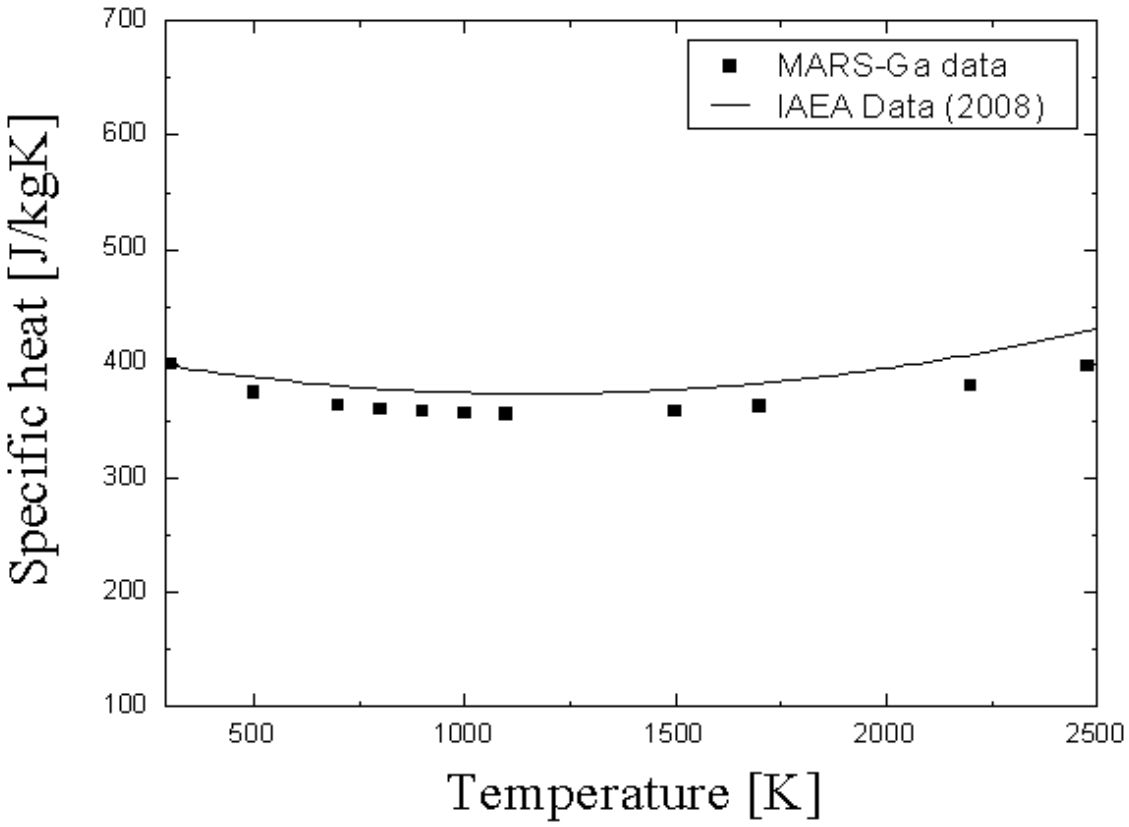

Fig. 2-4 Specific heat comparison of generated thermodynamic table data with IAEA report for gallium

Chapter 3. Experimental study of natural convection heat transfer using gallium properties

3.1 Introduction

The knowledge of the natural convection heat transfer in liquid gallium is important for an understanding of natural convection phenomena in liquids with low Prandtl numbers. Gallium belongs to group III of the periodic table of the elements. The melting temperature of liquid gallium is close to the room temperature, while its boiling temperature is about 2477 K. This is a prominent feature of gallium among various candidates for liquid-metallic coolants of nuclear applications[3].

Natural convection is a buoyancy-driven fluid motion that is able to function without electric power or actuation by control equipments. The natural convection-driven system provides several benefits such as simplicity, reduction of the cost and no usage of cooling pumps. In nuclear engineering, the so-called passive heat removal systems using natural convection play a key role for nuclear safety.

Therefore, this part of this study aims to experimentally investigate the heat transfer characteristics of liquid gallium in a rectangular loop under natural convection to secure experimental data of liquid gallium that are usable to the passive cooling systems of nuclear power plants or other liquid metal applications. Of course, although there have been many experimental data of natural convection in non-metallic fluids such as water, liquid metals such as sodium, LBE are few and those of gallium are fewer compared to other liquid metals.

3.2 Literature survey

There are several previous studies for the natural convection experiments that use liquid metals and gallium.

Hata et al[15]. obtained systematically the experimental data of natural convection heat transfer from a horizontal test cylinder in liquid sodium for Rayleigh number ranging from 41 to 25650 and examined whether the experimental results can be described and compared using existing correlations.

Jackson et al[16]. presented a theoretical model that was influenced of buoyancy on turbulent heat transfer to liquid sodium flowing in a vertical pipe. In this work, the equations for laminar and turbulent free convection to liquid sodium were obtained.

Davies et al[17]. described the sodium natural convection (SONAC) experiment for studying natural convection from a flat heater plate immersed in a sodium pool which can be inclined from the vertical to the horizontal with the heat flux in a downward direction. The experimental correlations for a horizontal position and 15 degree-inclined position in sodium were obtained.

Borgohain et al[18]. carried out not only the steady state natural circulation experimental studies of

LBE loop for different power levels but also transient studies for start-up natural convection, loss of heat sink and step power change in the loop. This study developed a 1D code named LeBENC to simulate the natural convection characteristics in closed loops and conducted validation of the LeBENC code with the experimental data and the results showed good agreements.

Ma et al[19]. designed and constructed the test facility to investigate the thermal hydraulic characteristics of LBE. The experiments showed that the maximum flow rate for the natural convection was up to 0.5 kg/s, resulting in the maximum heat removal of 15 kW from the core tank. The analysis performed with the RELAP5 code is in reasonable agreements with the results.

The circumferential distribution of the Nusselt number for mercury was reported by Michiyoshi et al[20]. This work presented the experimental data of natural convection heat transfer from a horizontal cylindrical heater immersed in mercury pool with the magnetic field and without the magnetic field. From experimental results, magnetic field affected local heat transfer coefficients and the local Nusselt number decreased with increasing the Hartmann number.

Two-dimensional convection of liquid metals below an infinite strip and axisymmetric convection below a circular plate was computed for a uniform surface temperature and for a uniform heat flux in Schulenberg[21]. The local Nusselt number was correlated with the Grashof and Prandtl numbers and it was predicted to be higher than those previously achieved with integral methods but agreed better with experiments.

Sugiyama et al[22]. clarified the heat transfer characteristics of natural convection around a horizontal circular cylinder immersed in liquid metals. This paper presented numerical results by using the Boussinesq approximation compared to existing experimental data for several liquid metals.

Hurle et al[23]. reported an experimental study of the occurrence of temperature oscillations in liquid gallium contained in a rectangular boat and heated from the side. This work indicted that the period of temperature oscillations increased as increasing boat length rather than depth and decreased as the effect of a transverse magnetic field. Additional result for this was provided by the fact that the onset of oscillations didn't produce a significant increase in the Nusselt number.

Mohamad et al[24]. attempted to combine experimental and full numerical simulations to gain improved understanding of some aspects of the flow and natural and mixed convection in a shallow rectangular cavity filled with liquid gallium. Temperatures were recorded at different locations in the cavity and temporal variation of the temperatures was analyzed. The results showed that lid motion had a significant effect on the flow and thermal structures in the cavity.

Derebail et al[25]. simulated two and three-dimensional modeling of temperature flow fields in test cell used for steady natural convection experiments in liquid gallium. Three different three-dimensional numerical models are compared to each other and to that of an experimental radioscopic visualization. The temperature contours of three-dimensional numerical model were in good

agreement with the experimental visualization.

Tagawa et al[26]. experimentally measured the heat transfer rate of natural convection in liquid gallium in a cubical enclosure under an external magnetic field applied horizontally and parallel to the vertical heated wall and the opposing cooled wall of the enclosure. Experiments were conducted in the range of modified Rayleigh number from 1.85×10^6 to 4.76×10^6 and Hartmann number from 0 to 573. The average Nusselt number was measured and found to increase when a moderate magnetic field was applied but to decrease under a stronger magnetic field.

Yamanaka et al[4]. reported an experimental investigation of the average rate of heat transfer as well as the oscillatory span-widths of the Nusselt number and the Rayleigh number in a layer of liquid gallium. These quantities were determined by measuring the instantaneous temperature difference between the upper and lower horizontal cooper plates. The time-averaged Nusselt number agreed well with the data for mercury at comparable values of the Rayleigh number.

Juel et al[27]. provided convincing numerical and experimental evidence for the importance of three-dimensional effects in free convective flow of liquid gallium in a rectangular enclosure of moderate aspect ratio. Agreement was demonstrated between experimental measurements and three-dimensional simulations of the convective heat transfer over an extended range of Grashof numbers for which the convective flow is steady. The amplitude of the vertical temperature profiles was plotted as a function of the Grashof number.

Xu et al[28]. presented an experimental study on temperature gradient induced natural convection in gallium. The obtained velocity and temperature distributions were compared with numerical simulations and reasonably good agreements were achieved.

Selver et al[29]. conducted an experimental study of natural convection in gallium enclosed by vertical circular cylinders with horizontal circumferential heating. Temperature measurements were made at six axial levels around the circumstance of the cylinder to study thermal convection. A numerical analysis was also conducted.

Kamotani et al[30]. showed the natural convection oscillation experiment of liquid gallium in cylinder heated from below for angles of inclination ranging from 0 to 75deg. The flow was found to become oscillatory beyond a certain Rayleigh number. The oscillations were associated with the back and forth motion of the basic unicellular structure and the oscillation amplitude was increased along the interface between the warm upflow and the cod downflow.

Table 3-1 showed these experimental or numerical correlations for several liquid metals.

Literature reviews of natural convection for several liquid metals have indicated that there were no natural convection heat transfer correlations for liquid gallium based on experimental results, in particular, for a rectangular loop which is typically adopted in a passive heat removal system.

3.3 Natural convection experiment

3.3.1 Natural convection rectangular test loop

The experiments were performed in a rectangular loop. The tubes of the test loop were made of stainless steel 316L with outer diameters of 1/2". The test loop was constructed based on the schematic design as shown in fig. 3-1 and fig. 3-2 shows the general view of the test loop. The indirect heating method of the test loop was adopted due to higher electric conductivity of gallium compared to water. The heater was formed by bolstering together four $10\,\text{mm} \times 445\,\text{mm}$ plate heaters between stainless steel 304 mass and there is a tube as a flow path of liquid gallium as shown in fig. 3-3 and 3-4. To measure the natural convection mass flow rate of liquid gallium, the dp transmitter for measuring differential pressures for an orifice was used. In the heater, there are eight 1.6 mm diameter K-type thermocouples to measure the temperature of heater, eight 3.2 mm diameter K-type thermocouples to measure the temperature of center of stainless steel mass and eight 1.6 mm diameter K-type thermocouples to measure the temperature of the surface of the flow path tube. By using these thermocouples, heat flux can be obtained and then calculate the heat transfer coefficient of liquid gallium with surface temperature in a flow path tube and the temperature of liquid gallium. To reduce the heat losses, the loop was insulated by 25 mm thickness glass wool except for the tube in tube type heat exchanger connected to the refrigerating bath circulator as shown in fig. 3-2(c). Before doing the experiment, the test loop was preheated using heating cables to raise the entire temperature in the loop over 303 K (30℃) because of the melting point of liquid gallium as shown in fig. 3-2(b). All operations were controlled by two electrical panels.

3.3.2 Experimental procedures

Gallium was melted by using hot plate to maintain its liquid-phase and then injected into the furnace. After finishing the injection, the gallium flowed to the heater through a vertical pipe and it traveled through the upper horizontal pipe and then flowed to the heat exchanger where it was cooled. The liquid gallium then left the heat exchanger and flowed to the orifice which was placed on the lower horizontal pipe. Finally, the natural convection experimental data were collected from thermocouples and dp transmitter in a data acquisition system and then saved to a computer.

3.3.3 Measurement uncertainty

The heat loss is estimated at ~ 12 % of the electrical power input. The heat flux was calculated by using temperature data in a heater. The uncertainty of the orifice and dp transmitter for measuring mass flow rate of liquid gallium are ± 1.7 % and 5% respectively. The uncertainty of temperature measurements are ± 0.5 %. The uncertainty in Nusselt number was 18-59 %.

3.4 Result and discussion

3.4.1 Capability of natural convection flow

It is essential to know the maximum natural convection flow rate in order to predict a heat removal limit or capability in a thermal-hydraulic system such as decay heat removal system of nuclear power plants. To investigate the capability of natural convection of liquid gallium in the test loop, the flow rates were measured. Before doing the experiment, several prediction methods were used to compare the mass flow rates of liquid gallium.

3.4.1.1 Prediction of the mass flow rate with an existing correlation

Under natural convection conditions, the test loops operate without a pump and the flow is driven entirely by the buoyancy-generated power. The density dependence on temperature can be assumed linear so that in general[31]:

$$\rho = \rho_0 \left[1 - \beta \left(T - T_0 \right) \right] \tag{3.1}$$

In natural convection conditions, the buoyancy pressure and frictional pressure drop are considered.

$$\Delta P_B = \left(\rho_{in} - \rho_{out} \right) g \Delta L = \beta \rho_0 \Delta T_H g \Delta L \tag{3.2}$$

$$\Delta P_f = C_R \frac{\dot{m}^n}{2\rho_l} = \frac{1}{2} R \frac{\left(\dot{m} \right)^{2-n}}{\rho_l} \tag{3.3}$$

Under natural convection conditions, the momentum equation can be reduced to :

$$\Delta P_f = \Delta P_B \tag{3.4}$$

Substituting from eq. (3.2) and (3.3) into eq. (3.4) and assuming that the temperature variation round the loop is such that the density variation is relatively small so that $\rho_0 \cong \rho_l$,

$$\frac{1}{2} R \frac{(\dot{m})^{2-n}}{\rho_0} = \beta \rho_0 \Delta T_H g \Delta L \tag{3.5}$$

Therefore, for a given temperature difference the mass flow rate may be obtained and anticipated before doing the experiment[32].

$$\dot{m} = \left[\frac{2\beta \rho^2 g \Delta H q}{C_p R} \right]^{1/3} \tag{3.6}$$

where the total hydraulic resistance, R is given by

$$R = \frac{L_t}{D} \frac{P}{\mathrm{Re}_{ss}^b} \frac{1}{A^2} \sum_{i=1}^{N} \left(\frac{\ell_{eff}}{D^{1+b} A^{2-b}} \right) \tag{3.7}$$

where L_t is the total length of test loop, b is the constant (laminar :1, turbulent : 0.25), P is the constant (laminar : 64, turbulent : 0.316).

$$\mathrm{Re}_{ss} = 1.96 \left[\frac{Gr_m}{N_G} \right]^{1/2.75} \tag{3.8}$$

where N_G is a geometric parameter defined as

$$N_G = \frac{L_t}{D} \sum_{i=1}^{N} \left(\frac{\ell_{eff}}{D^{1+b} A^{2-b}} \right) \tag{3.9}$$

where Gr_m is a modified Grashof number and ℓ_{eff} is L_{eff}/L_t.

3.4.1.2 Prediction of the mass flow rate with CFD analysis

In this part, flow and temperature distributions were analyzed applying computational fluid dynamics (CFD) as shown in fig. 3-5. The simulation was done in a 3D geometry and the modeling simplification was divided by a heater, a heat exchanger and two horizontal parts instead of a full geometry description by addressing only the fluid region with appropriate boundary conditions such as heat flux in a heater and heat exchanger while the boundary conditions of two horizontal parts were the adiabatic condition. The basic gallium properties according to a reference temperature were entered as one of the information for materials. The changes of mass flow rate of liquid gallium in the CFD analysis agreed well with the experimental results as shown in fig. 3-7.

3.4.1.3 Prediction of the mass flow rate with MARS-Ga analysis

The comparison of the experimental data with computer code analysis is an important function for the validation of the models employed in the codes and furthering the application. In this part, MARS-Ga code was also used to analyze the thermal-hydraulic characteristics of the test loop. By using this thermodynamic property table file, tpfga, the thermal hydraulic systems of liquid gallium can be simulated for numerical and parametric studies. Fig. 3-6 indicates the nodalization of the test loop. Fig. 3-7 shows the comparisons of the experimental data with eq. (3.6), CFD and MARS-Ga according to a level of the input power. The maximum mass flow rate is about 0.037 kg/s for the maximum heat flux and the predictions show good agreements with the experimental data.

3.4.2 Capability of natural convection heat transfer

Fig. 3-8 shows the correlation of the non-dimensional numbers, Nusselt and Rayleigh number. By averaging the local surface temperatures of the flow path tube, average temperature and the average heat transfer coefficients of liquid gallium were obtained. Average Nusselt numbers were derived from the average heat transfer coefficients and all points of averaged Nusselt numbers were calculated within the heat flux range of 6.17×10^3 to 5.07×10^4 W/m^2. From the experimental data, the present study obtained a correlation for the laminar natural convection heat transfer in a rectangular loop of liquid gallium as follows :

$$Nu_D = 0.745 + 0.004 Ra_D^{0.033} \approx 0.75 \qquad (3.10)$$

where $3.74 \times 10^3 \leq \mathrm{Ra_D} \leq 2.68 \times 10^4$.

The experimental data of average Nusselt numbers are 2 and 4 times lower than the values given by Schulenberg[21] and Sugiyama et al[22]. respectively.

3.5 Conclusion

The study on natural convection capability of gallium was carried out in a rectangular loop consisted of stainless steel 316L tube. For natural convection experiment, the heater for liquid gallium was designed and constructed. To check the heat flux, twenty K-type thermocouples were used in a heater. During the experimental process, steady state natural convection for gallium observed within the heat flux range of 6.17×10^3 to 5.07×10^4 $\mathrm{W/m^2}$. From the experimental observations, mass flow rate of liquid gallium was obtained by measuring the differential pressure of liquid gallium using orifice and dp transmitter and heat average heat transfer coefficients can be calculated by measuring the surface temperature of the flow path and the temperature of liquid gallium from thermocouples. The experimental data of average Nusselt numbers are 3 and 4 times lower than the values given by Schulenberg[21] and Sugiyama[22] et al. respectively.

A numerical code, MARS-Ga was developed to predict the behavior of gallium in the loop and was validated against the experimental results. It was found that the predictions are in good agreements of the trend with the experimental results as well as CFD analysis.

Table 3-1. Experimental or theoretical correlations of Nusselt numbers for heat transfer to several metals.

Authors	Working fluid	Correlations
Jackson et al. [5]	Sodium	$Nu = 0.675\left(Gr \cdot \mathrm{Pr}^2\right)^{0.25},\ \left(Gr\,\mathrm{Pr}^2 \le 10^6\right)$ $Nu = 5 + 0.4\left(Gr \cdot \mathrm{Pr}^2\right)^{0.3},\ \left(2\times10^5 \le Gr\,\mathrm{Pr}^2\right)$
N.W. Davies et al. [6]	Sodium	$Nu = 1.19\left(0.522 - 0.0437\,\mathrm{Pr} - 0.0673\,\mathrm{Pr}^2\right)\left(Gr \cdot \mathrm{Pr}^2\right)^{1/6}$ $\left(0.001 \le \mathrm{Pr} \le 0.1\right)$
Michiyoshi et al. [9]	Mercury	$Nu = 0.53\left(Gr \cdot \mathrm{Pr}^2\right)^{1/4}$ $Nu = 0.571\left(Gr \cdot \mathrm{Pr}^2\right)^{1/5}$ $Nu = 0.643\left(Gr^* \mathrm{Pr}^2\right)^{1/6}$
T. Schulenberg [10]	Liquid metals	$Nu = 0.705\left(Gr \cdot \mathrm{Pr}^2\right)^{1/5}$ $Nu = 0.776\left(Gr^* \mathrm{Pr}^2\right)^{1/6}$ $\left(\mathrm{Pr} \le 10^{-2}\right)$
K. Sugiyama et al. [11]	Liquid metals	$Nu_m = 1.11\left(Gr \cdot \mathrm{Pr}^2\right)^{0.196}$ $\left(4 \le Gr\,\mathrm{Pr}^2 \le 7000\right), \left(0.004 \le \mathrm{Pr} \le 0.02\right)$
R. Derebail et al. [14]	Gallium	Two dimensional Model: $Nu_{av} = 0.083 + 0.052Gr^{0.293}$ Three dimensional Model: $Nu_{av} = 0.882 + 9.312\times10^{-7}Gr^{0.909}$ $\left(Gr < 1.6\times10^7\right)$

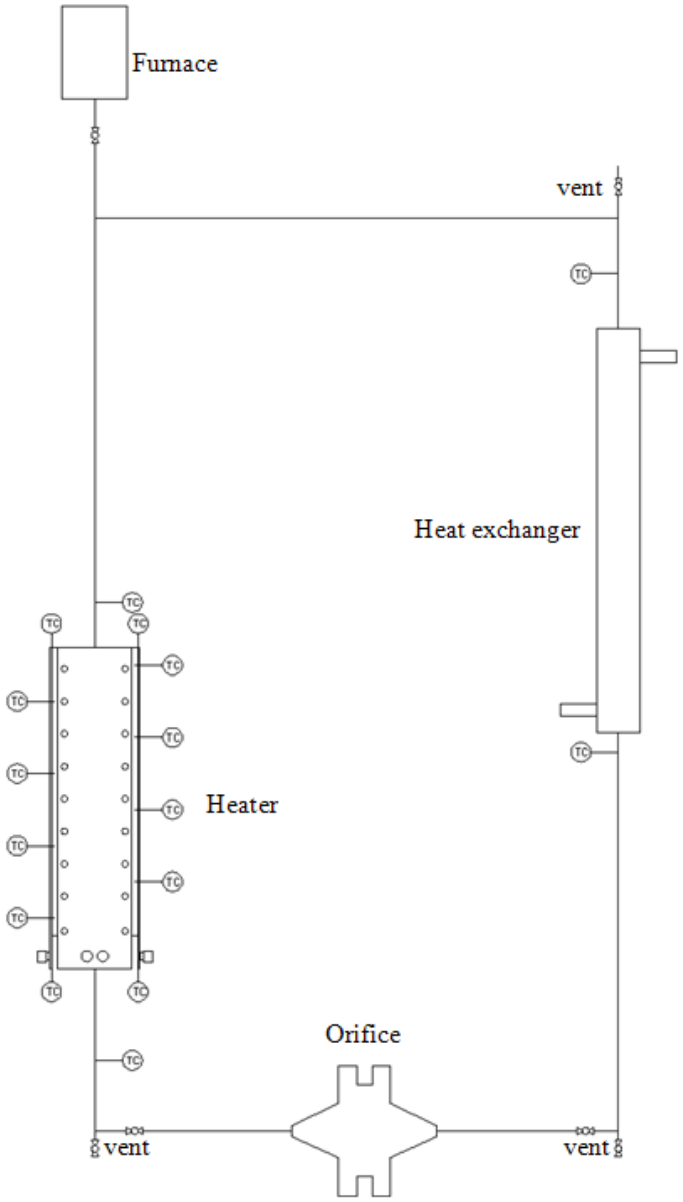

Fig. 3-1 Schematic of the test loop

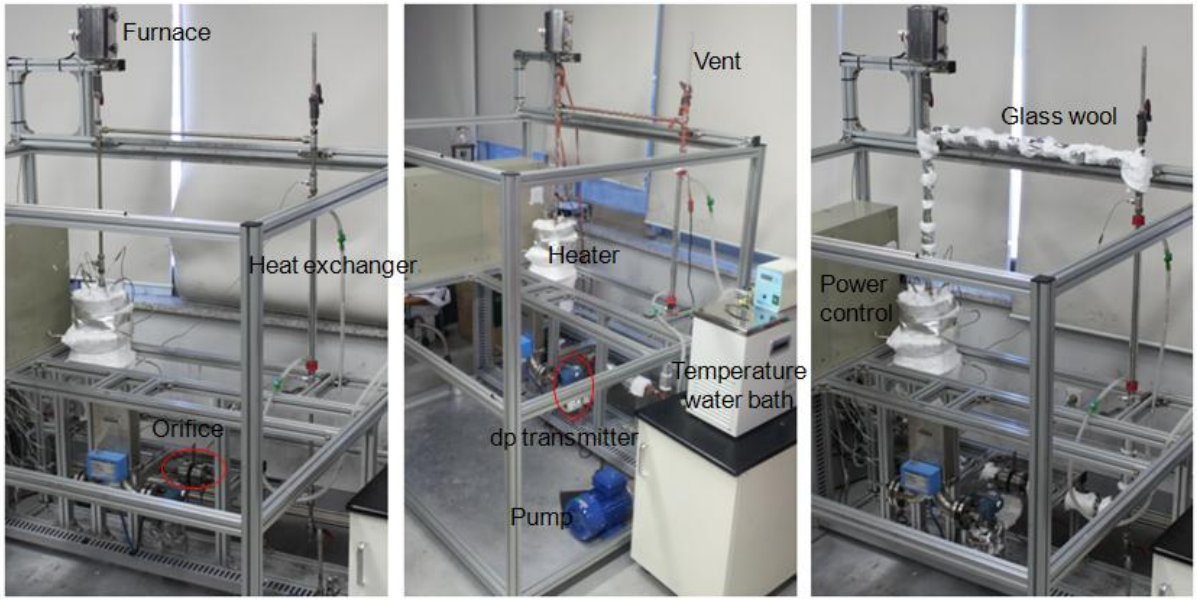

(a) (b) (c)

Fig. 3-2 The natural convection loop : (a) the general view, (b) with heating cables, (c) with ceramic wool

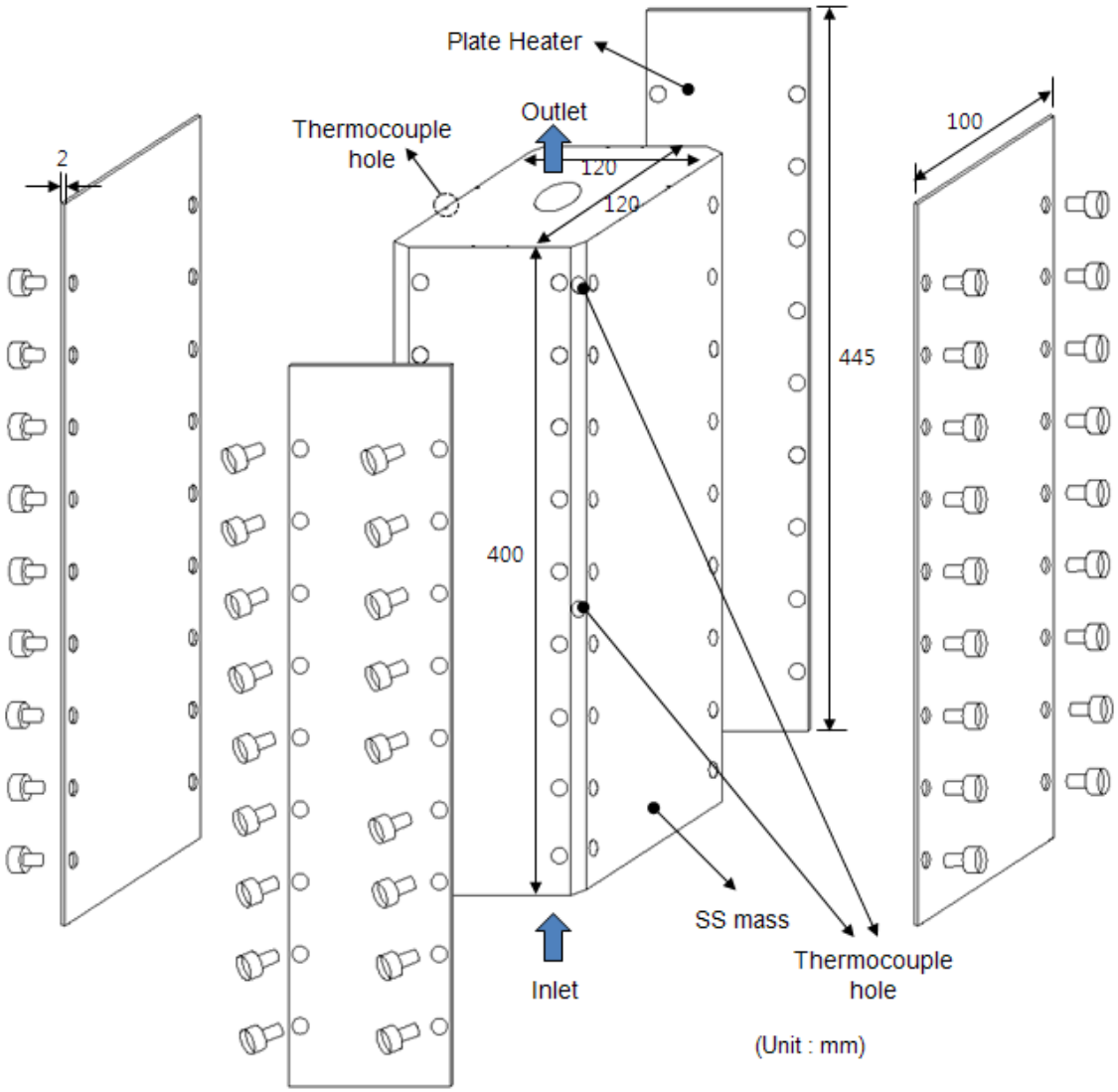

Fig. 3-3 Construction of the heater assembly

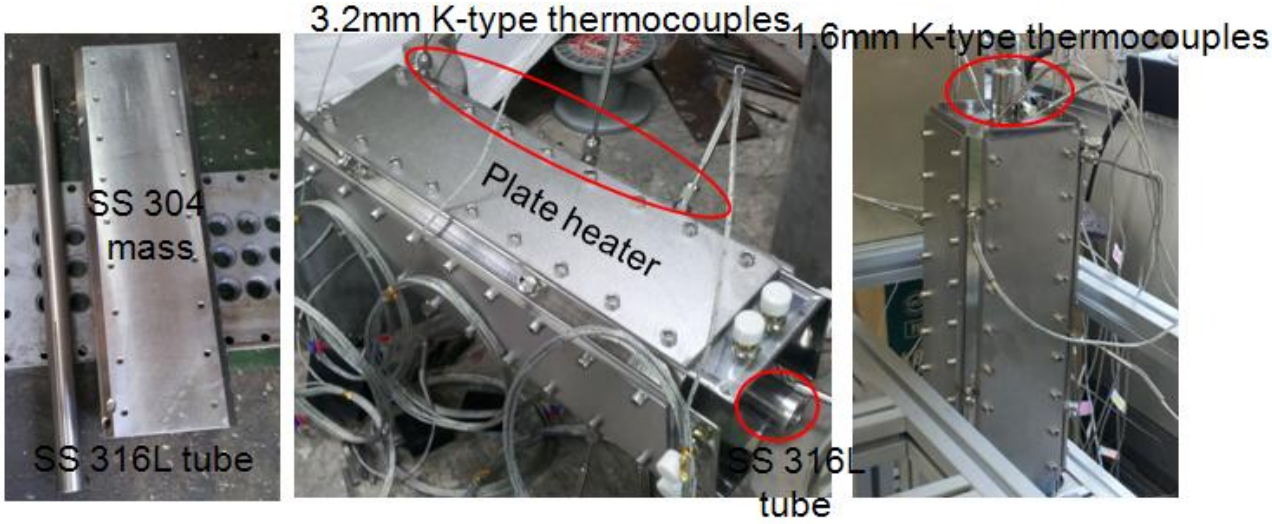

(a) (b) (c)

Fig. 3-4 Heater for liquid gallium : (a) SS 304 mass, (b) with thermocouples and plate heaters, (c) connected the test loop

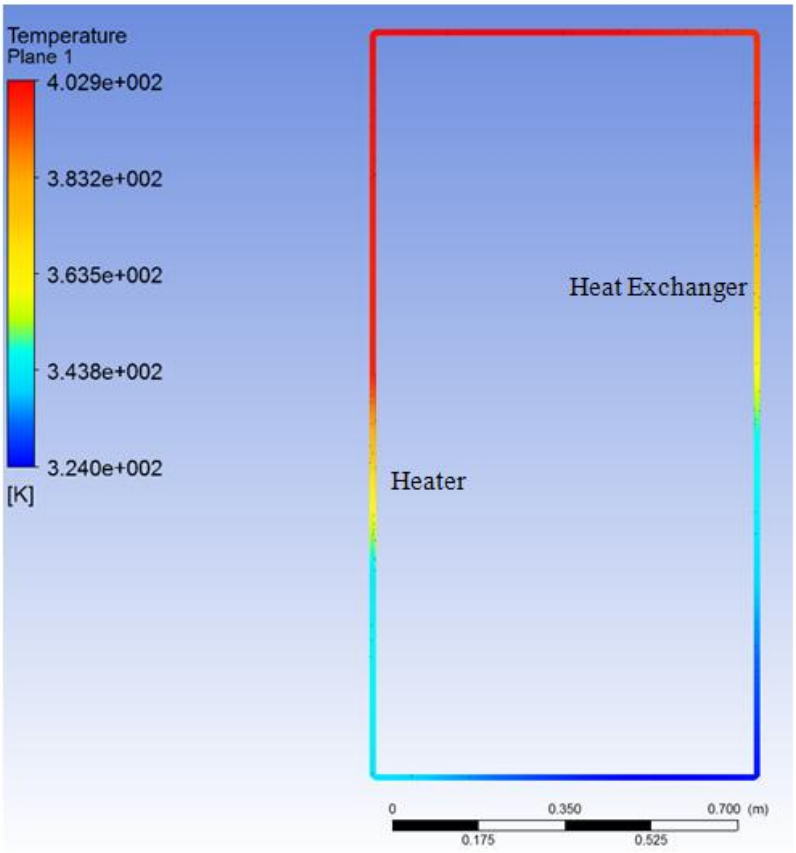

Fig. 3-5 Temperature contours in the test loop for natural convection

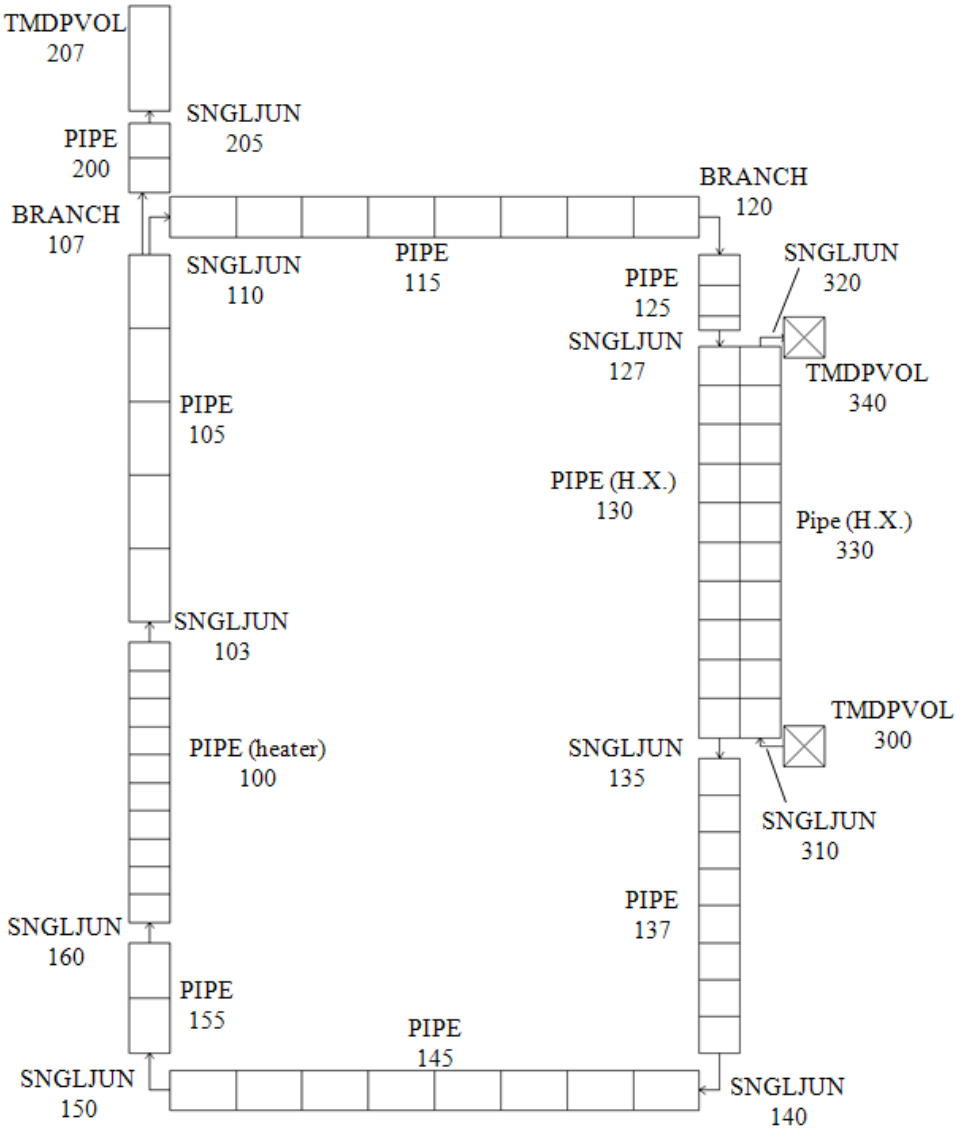

Fig. 3-6 Nodalization of the test loop adopted for MARS-Ga

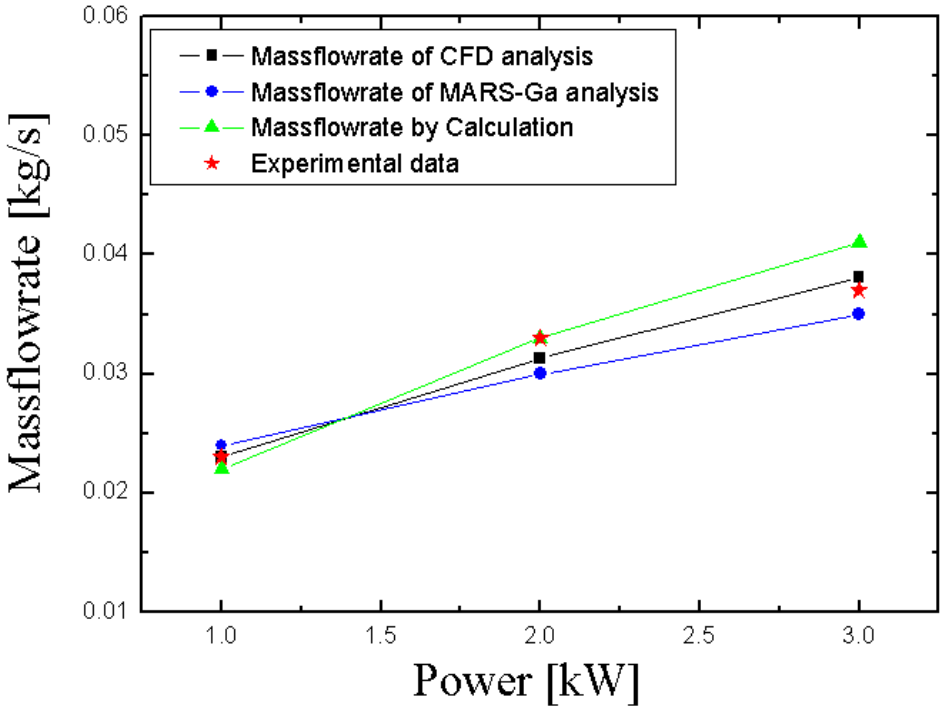

Fig. 3-7 Comparison of the experimental results with an existing correlation, CFD and MARS-Ga

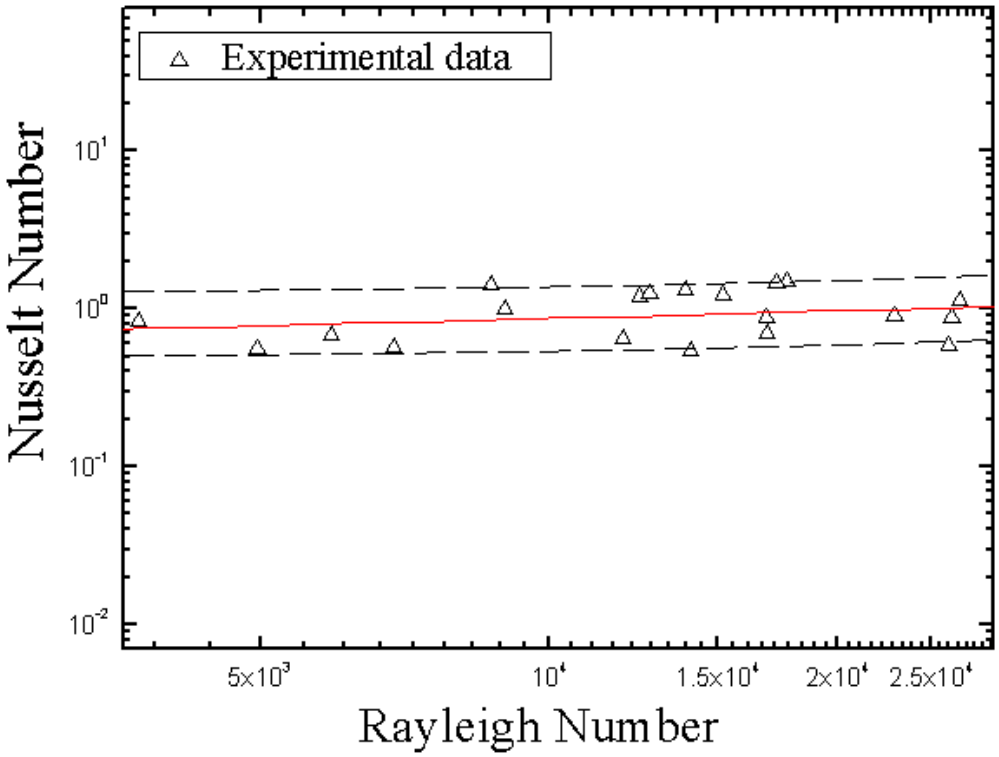

Fig. 3-8 Average Nusselt numbers on the surface of the flow path tube for Rayleigh numbers of liquid gallium

Chapter 4. Numerical study of in-vessel retention under the gallium-water external reactor vessel cooling system using MARS-Ga

4.1 Introduction

IVR-ERVCS (In-Vessel corium Retention through External Reactor Vessel Cooling System) is known to be an effective method for mitigating severe accident in nuclear power plants. It maintains the integrity of the reactor vessel when a severe accident occurs[33] and has been adopted in several light water reactors such as AP 600, AP 1000 and APR 1400.

To confirm the feasibility of the gallium-water IVR-ERVCS to solve the limitation due to critical heat flux in IVR-ERVCS and to ensure the sufficient thermal margin, the numerical analyses using MARS-GA were performed to investigate its temperature distribution and the working time. Furthermore, sensitivity studies related to the initial temperature of liquid gallium and the inventory of the water pool, which acts as a heat sink, were also conducted.

4.2 Literature survey

Many studies of water-cooled reactors have been performed, for example, Kang et al[33]. analyzed the flow behavior inside the reactor pressure vessel insulator of OPR 1000. It was found that in the cases of large break loss of coolant accident (LBLOCA) and station black out (SBO), water ingression and steam venting through the insulator are critical factors for the effective cooling via boiling heat removal at the outer surface of the reactor pressure vessel.

To simulate the in-vessel retention of VVER-440/V213, model improvements and adaptations of the ASTEC (Accident source term evaluation code) were employed by the CEA in France[34].

The external cooling of the reactor wall was simulated by applying imposed coolant temperature and heat transfer coefficient, and the obtained results were found to be in good agreement with available predictions from other codes, particularly the shape and depth of ablation and the maximum heat flux in case of a thick metallic layer.

Mladin et al[35]. studied the debris bed interaction with the calandria vessel following an accident with severe core degradation in a CANDU reactor, using a modification of the RELAP5/MOD3.4 code. The coolability of the calandria vessel starting with a dry debris bed was investigated, and it was confirmed that the shield tank water was capable of removing heat from the calandria vessel wall, as long as the liquid phase was present in the tank. The authors also compared the vessel rupture time to the calculated value for a LOCA (Loss of coolant accident) with loss of all heat sinks and no recovery actions and performed parametric studies to quantify the effects of several identified sources of

uncertainty.

Studies of the IVR-ERVCS in small integral reactors have also been conducted. For example, to evaluate the in-vessel retention of a small integral reactor, Park et al[36]. perfomed a thermal load analysis from the corium pool to the outer reactor vessel wall in the lower plenum of the reactor vessel, to determine the heat flux distribution. The thermal margin was evaluated by comparing the thermal load, on the outer reactor pressure vessel wall, with the maximum heat removal rate at the critical heat flux (CHF). The water circulation mass flow rate between the outer reactor pressure vessel and the insulation was obtained as a function of heat flux and water inlet area from RELAP5/MOD3 results which confirmed that the reactor pressure vessel integrity is maintained by the IVR-ERVCS.

To propose enhanced designs for the coolant inlets and upper steam-venting slots in the insulation of APR 1400, the large-scale air injection experiment was performed by Park et al[37]. Steady-state simulations of this experiment using RELAP5/MOD3 code were also carried out to verify the experimental data and to investigate the coolant behavior between the reactor pressure vessel wall and the insulation material. The simulated values of the water circulation mass flow rate from RELAP5/MOD3 were found to be very similar to the experimental results. Although significant research has been conducted to enhance the IVR-ERVCS, it is not yet certain whether it has a sufficient thermal margin for use in nuclear power plants with higher thermal power.

The IVR-ERVCS also has a limitation on the CHF during the decay heat removal by water flooded into the cavity. To avoid this heat removal limit of CHF during boiling of water, Park & Bang[38] introduced a new approach by changing the flooding material from borated water to liquid metal, gallium. This research suggested that the favorable properties of liquid gallium such as low melting point, high boiling point, and no reaction with water, ensure that it can play an important role in nuclear safety as an alternative coolant in the gap between the vessel and vessel insulation. In this research, two concepts of the gallium-water IVR-ERVCS were designed and simulated by a CFD analysis. It was found that the temperature range of these systems was below the boiling point of the gallium, and therefore the natural convection of the gallium can be expected to be stable and continual.

4.3 MARS-Ga modeling of gallium-water IVR-ERVCS

Fig. 4-1 illustrates the side-cooling concept, where two fluids are separated by a block structure[38]. The block structure divides the gallium and water regions and acts as a second vessel or liquid metal catcher. To reduce the heat loss during normal operation, insulation was used between the reactor vessel and the block structure, instead of between the reactor vessel and the cavity. Gallium floods into the liquid metal catcher by the action of gravity, and water also floods into the cavity in the same

way. The decay heat generated in the corium is transferred to liquid gallium through the reactor pressure vessel and then to the water pool, which acts as a heat sink, via the liquid metal catcher.

Numerical analyses of the gallium-water IVR-ERVCS in APR 1400 were performed using MARS-Ga. Fig. 4-2 compares the reactor vessel cavity arrangement of APR 1400 and the nodalization of the existing and the gallium-water IVR-ERVCS, and table 4-1 lists the initial conditions and geometry information used in the MARS-Ga analysis.

The dimension between the insulator and structure (SV253-SV305) refers to the design of Park & Bang[38]. Stainless steel was selected as the material of structure between liquid gallium and water, and it is assumed that the initial temperatures of liquid gallium and water are 313.15 K (40˚C). In the nodalization, the flow path of liquid gallium between the reactor pressure vessel and insulator (SV100-SV153) and between the insulator and structure (SV253-SV305) were composed of single volumes (SV). The water pool was also composed of single volumes (SV579-SV627). TDV801 is the time-dependent volume (TDV) that vents the generated steam from the water pool. The flow path of liquid gallium and the borated water pool were connected with single junctions having a cross flow.

In this research, a medium break loss-of-coolant accident (MBLOCA) of 4.28" break size in the cold leg, without actuation of the safety injection pumps, but with effective actuation of the safety injection tank (SIT) was simulated from transient initiation to reactor vessel failure[39-40]. At the initial stage, the decay heat increases to 0.45 – 2.2 MW/m^2 in 20 s.

4.4 Result and discussion

4.4.1 Temperature distribution under MBLOCA

The analysis was focused on the range of temperatures on the outer reactor pressure vessel wall and in the liquid gallium. The surface temperature distribution in the reactor vessel is shown in fig. 4-3. The initial temperature of the reactor vessel was between 322.15 K (49˚C) and 340.15 K (67˚C) and the temperature after heat removal for 3.8 h was in the range from 448.15 K (175˚C) to 565.15 K (292˚C). The initial temperature of liquid gallium was about 313.15 K (40˚C) and the temperature after 3.8 h was in the range from 373.15 K (100˚C) to 402.15 K (129˚C), as shown in fig. 4-4. The analyses confirmed that the maximum temperature of liquid gallium in the cavity was below the boiling point of gallium and that natural convection flow occurs in the gallium and water regions. Although the results obtained using the MARS-Ga have lower values compared to those in Park & Bang[38], the temperature range was in a good agreement. The simulation was also performed for the water-water IVR-ERVCS with the same geometry and showed that the surface temperature

distribution in this reactor vessel was slightly lower than that of the gallium-water IVR-ERVCS. Table 4-2 indicates the entire temperature distributions in the gallium-water IVR-ERVCS and water-water IVR-ERVCS. Because the specific heat of liquid gallium is lower than that of water, the temperature range of liquid gallium was higher than that of water. However, this does not matter as the boiling point of liquid gallium is much higher than that of water. Fig. 4-5 shows the mass flow rate of the coolants in the gallium-water IVR-ERVCS and water-water IVR-ERVCS. The junctions in this figure indicate the connection from SV 100 to SV 109. Because the gallium-water IVR-ERVCS doesn't have a phase change, the gallium level in the cavity and the void fraction do not change, unlike the water level and void fraction in the water-water IVR-ERVCS, as demonstrated in fig. 4-6. This is the main advantage of the gallium-water IVR-ERVCS in terms of safety margin.

4.4.2 Heat transfer coefficient

In the MARS-Ga, the appropriate convective correlations were used according to the heat transfer mode and geometry. Because the gallium-water IVR-ERVCS operates in the single phase liquid convection mode, the Churchill-Chu[41], McAdams, and Sellars correlations were calculated and their maximum value was used in the simulation. The Churchill-Chu correlation that may be applied over the entire range of Rayleigh number, as shown in eq. (4.1) was used for the gallium-water IVR-ERVCS.

$$Nu_L = \left\{ 0.825 + \frac{0.387 Ra_L^{1/6}}{\left[1 + \left(\frac{0.492}{\mathrm{Pr}} \right)^{9/16} \right]^{8/27}} \right\}^2 \qquad (4.1)$$

$$Nu_L = 0.27 Ra_L^{0.25} \qquad 10^5 < Ra_L < 10^{10} \qquad (4.2)$$

$$Nu = 4.36 \qquad (4.3)$$

Unlike the gallium-water IVR-ERVCS, the water-water IVR-ERVCS has change in the heat transfer mode from the single-phase natural convection to subcooled nucleate boiling, as shown in fig. 4-7, and therefore the Churchill-Chu and Chen correlations represented by eq. (4.1) and eq. (4.4) – (4.6), respectively, are used for its simulation[42]. Table 4-3 indicates the numbers corresponding to different heat transfer modes, used in the MARS-Ga.

$$q'' = h_{mac}\left(T_{wall} - T_{spt}\right) + h_{mic}\left(T_{wall} - T_{spt}\right)S \tag{4.4}$$

$$h_{mac} = 0.023\,\mathrm{Re}_L^{0.8}\,\mathrm{Pr}_L^{0.4}\left(k_L / D\right)F \tag{4.5}$$

$$h_{mic} = 0.00122\left(\frac{k_f^{0.79} C_{pf}^{0.45} \rho_f^{0.49}}{\sigma^{0.5} \mu_f^{0.29} h_{fg}^{0.24} \rho_g^{0.24}}\right)\left(T_{wall} - T_{spt}\right)^{0.24} \Delta P^{0.75} \tag{4.6}$$

where T_{wall} and T_{spt} are the wall temperature and steam saturation temperature based on total pressure, respectively. k_f, C_{pf}, ρ_f, σ, μ_f, and h_{fg} are the thermal conductivity, specific heat, density, surface tension, viscosity, and enthalpy of vaporization of the fluid, respectively, and ρ_g is the density of the vapor. The Chen correlation uses the Dittus-Boelter correlation, with a Reynolds number factor F, for the convection heat transfer and the Forster-Zuber pool boiling correlation[43], with a suppression factor S, for the boiling heat transfer.

The range of the heat transfer coefficient of liquid gallium is 2000 – 21400 W/m^2·K as mentioned in table 4-2. Although the heat transfer coefficient of the single-phase liquid, gallium is lower than boiling heat transfer coefficient of water, the liquid gallium can be maintained at the steady state condition because it does not undergo a phase change unlike water, which has a rapid change or drop in the heat transfer coefficient when its level decreases after the phase change.

4.4.3 Critical heat flux

To confirm sufficient margins of CHF or no CHF occurrence in the water-water IVR-ERVCS compared to the gallium-water IVR-ERVCS, higher heat fluxes of up to 3200 W/m^2·K due to a LBLOCA of 9.6" break size in the cold leg, without actuation of the safety injection pump, were imposed on the heat structures[39-40]. In order to evaluate the newly-proposed ERVCS, simulation of the existing IVR-ERVCS of APR 1400 was also performed as a reference study, as shown in fig.4-2(b). The MARS-Ga uses the 1986 AECL-UO critical heat flux lookup table[44], which was made from tube data normalized to a tube inside diameter of 0.008 m and has factors that can be applied to allow its use for tube sizes or rod bundles.

$$\mathrm{CHF} = \mathrm{CHF}_{\text{lookup table}} \times K_{hy} K_{bf} K_{sp} K_{hl} K_{nu} K_{hor} K_{ver} \tag{4.7}$$

After obtaining CHF from the lookup table, the multiplying factors shown in eq. (4.7) are used to

compensate for differences in the heated length geometry, bundle geometry, spacer grid, heat flux profiles, and low flow condition. The seven correction factors such as K_{hy}, K_{bf}, K_{sp}, K_{hl}, K_{nu}, K_{hor}, and K_{ver} are the hydraulic diameter factor, bundle factor, grid spacer factor, heated length factor, axial flux distribution factor, horizontal flow factor, and vertical factor, respectively[45]. The value of critical heat flux was calculated for the range of heat transfer modes ranging from the subcooled nucleate boiling to saturated transition boiling.

Fig. 4-8 shows the wall temperature distribution in the outer reactor vessels of the existing, gallium-water, and water-water IVR-ERVCS under the LBLOCA, whereas the mass flow rate of coolants in the three systems are shown in fig. 4-9. The oscillation of water in the existing and water-water IVR-ERVCS was confirmed. Because liquid gallium has a high boiling point, there is no phase change phenomenon in the gallium-water IVR-ERVCS, and therefore sudden changes in the temperature and void fraction do not occur as in the existing and water-water IVR-ERVCS, as shown in fig. 4-8 and 4-10. To check the simulation process for predicting the CHF, the heat transfer mode change of the MARS-Ga was used. With increasing power, the wall temperature of the reactor vessel increased over 100 K more than saturated temperature, and the heat transfer mode changed from nucleate boiling to subcooled film boiling, as shown in fig. 4-11. At that moment, the void fraction and the water temperature are too low and the calculated CHF data from Greoneveld et al[44]. is higher than the given heat flux (~3200 kW/m^2) in the subcooled transition boiling mode. In other words, the reason of the sudden change in the wall temperature in the water-water IVR-ERVCS is not that the maximum heat flux is over the calculated CHF data from Greoneveld et al[44]. However, in the existing IVR-ERVCS, the heat transfer mode changed because the wall temperature is over 100 K more than the saturated temperature, as was observed by following up the flow chart of the CHF module in the code. With the change in the heat transfer mode, the heat transfer coefficient suddenly drops, and therefore the increase in wall temperature occurs according to the heat balance in the MARS-Ga. In gallium-water IVR-ERVCS, there were no temperature increases, implying no CHF occurrence or sufficient CHF margin, as expected.

4.4.4 Sensitivity studies

4.4.4.1 Initial temperature of coolant

The initial temperature of liquid gallium and water are 313.15 K (40˚C) as mentioned in table 4-1. In the sensitivity study of initial temperature of the coolant, the cases of 338.15 K (65˚C) and 363.15 K (90˚C) were simulated. In the case of 363.15 K (90˚C), the initial temperature of water had a strong influence on the working time of the cooling system because the void fraction increased more

compared to the other cases of water-water IVR-ERVCS, as shown in fig. 4-12. On the other hand, the gallium-water IVR-ERVCS with initial temperature of 365.15 K did not show a large difference compared to the base case (313.15 K, 40˚C). Therefore, it was inferred that, even at a higher initial temperature of liquid gallium, the gallium-water IVR-ERVCS could provide a stable cooling capability in severe accidents.

4.4.4.2 Size of the water pool as a heat sink

To know the effect of the size of the borated water pool in the gallium-water IVR-ERVCS, the pool size was varied and the simulations were carried out for each condition, as shown in fig. 4-13. In this part, the inventory of the water pool was controlled from 47 to 60 ton. Increasing the inventory of water in the water pool causes only a small change in the water level. It was observed that increase in the amount of water in the pool leads to an increase in the working time, because the water pool is a heat sink in the gallium-water IVR-ERVCS.

4.5 Conclusion

To investigate the feasibility of the gallium-water IVR-ERVCS based on Park & Bang[38], numerical simulations of severe accidents in an APR 1400- like geometry was performed using MARS-Ga as the system analysis code. The gallium-water IVR-ERVCS uses liquid gallium and water as coolants. The decay heat generated in the corium is transferred to the liquid gallium through the reactor pressure vessel and then removed from the water pool, which acts as a heat sink. In this study, the configuration used for the numerical simulation was the side-cooling concept, where the two fluids (liquid gallium and water) are separated by a block structure, which serves as a liquid metal catcher. To analyze the gallium-water IVR-ERVCS, the MARS-Ga with gallium properties was used, and the base geometry referred to the APR 1400 and design of Park & Bang[38]. The main consequence of the simulations is the confirmation of heat removal without CHF occurrence by the gallium-water IVR-ERVCS, a long as the liquid phase is maintained in the water pool. The maximum temperature of the liquid gallium was about 402.15 K (129˚C) showing that the liquid gallium has the potential to be a coolant in the IVR-ERVCS. Sensitivity studies for the gallium-water and water-water IVR-ERVCS were performed and compared. Through these studies, the influences of the initial temperature and the amount of water in the pool were analyzed, and it was found that the working time of the gallium-water IVR-ERVCS depends on the inventory of the water pool. Although the heat transfer performance of single-phase liquid gallium is lower than that of boiling water, in terms of the heat

transfer coefficient at the initial stage, the absence of phase change in the liquid gallium is an advantage of liquid gallium in terms of the CHF margin. This implies that the gallium-water IVR-ERVCS can provide stable and reliable cooling during severe accidents in nuclear power plants. To solve the limitation due to CHF of the existing IVR-ERVCS and to ensure sufficient thermal margin, the results of this study suggest that the gallium-water IVR-ERVCS can be a successful strategy for mitigating severe accidents in higher power-capacity nuclear power plants.

Table 4-1. Geometry of APR 1400 and initial conditions used in MARS-Ga analysis

Geometry and initial condition	Correlations	
Height [m]	7.4	
Radius of reactor vessel [m]	2.574	
Thickness of reactor vessel [m]	0.165	
Thickness of insulator [m]	0.114	
Thickness of barrier [m]	0.05	
Material of barrier of liquid-metal catcher	Stainless steel	
Initial temperature of gallium [K]	313.15 (40°C)	
Initial temperature of H_2O [K]	313.15 (40°C)	
Total amount of gallium [kg]	7.04×10^5	
Total amount of H_2O [kg]	1.8×10^5	
Heat flux [MW/m^2] under MBLOCA	$0° \leq \theta \leq 30°$	0.45
	$30° < \theta \leq 50°$	0.85
	$50° < \theta \leq 70°$	1.3
	$70° < \theta \leq 90°$	2.2

Table 4-2. Comparison of the gallium-water and water-water IVR-ERVCS

	Gallium	Water
Surface temperature of reactor vessel [K]	322 – 565	340 – 484
Coolant temperature [K]	313 – 402	313 – 375
Heat transfer coefficient [$W/m^2 \cdot K$]	~ 21400	~ 19600
Heat transfer mode	Single phase Natural convection	Single phase natural convection ↓ Subcooled nucleate boiling

Table 4-3. Heat transfer modes in the MARS-Ga

Mode	Conditions
0	Convection to noncondensable-steam-water mixture
1	Convection at supercritical pressure or superheat wall with negative heat flux due to superheated gas
2	Single-phase liquid convection at subcritical pressure, subcooled wall, and void fraction
3	Subcooled nucleate boiling
4	Saturate nucleate boiling
5	Subcooled transition boiling
6	Saturated transition boiling
7	Subcooled film boiling
8	Saturated film boiling
9	Single-phase vapor or supercritical two-phase convection
10	Condensation when void is less than one
11	Condensation when void is one

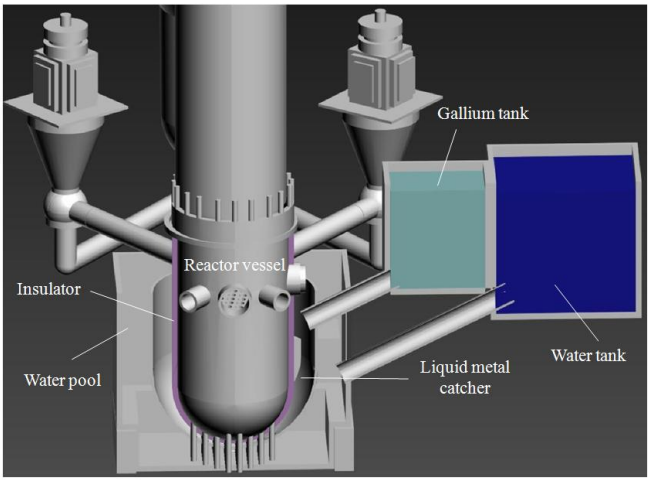

(a)

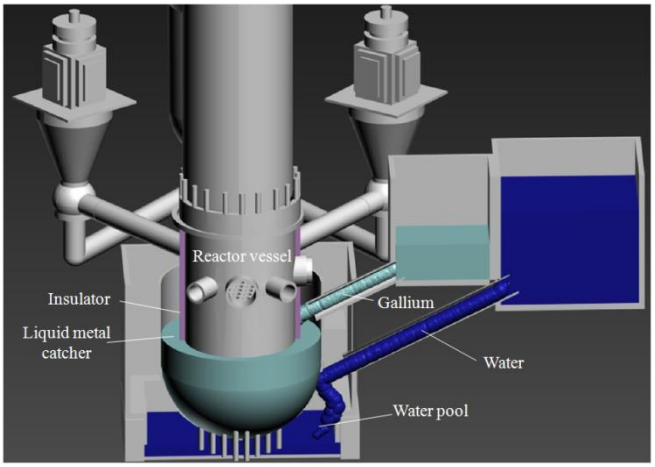

(b)

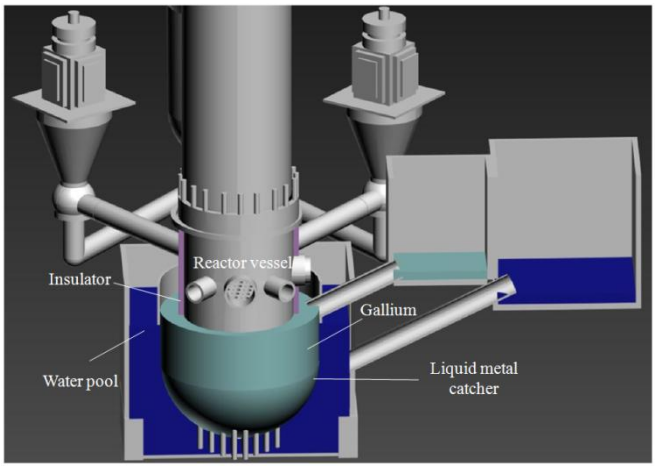

(c)

Fig. 4-1 Illustration of the gallium-water IVR-ERVCS

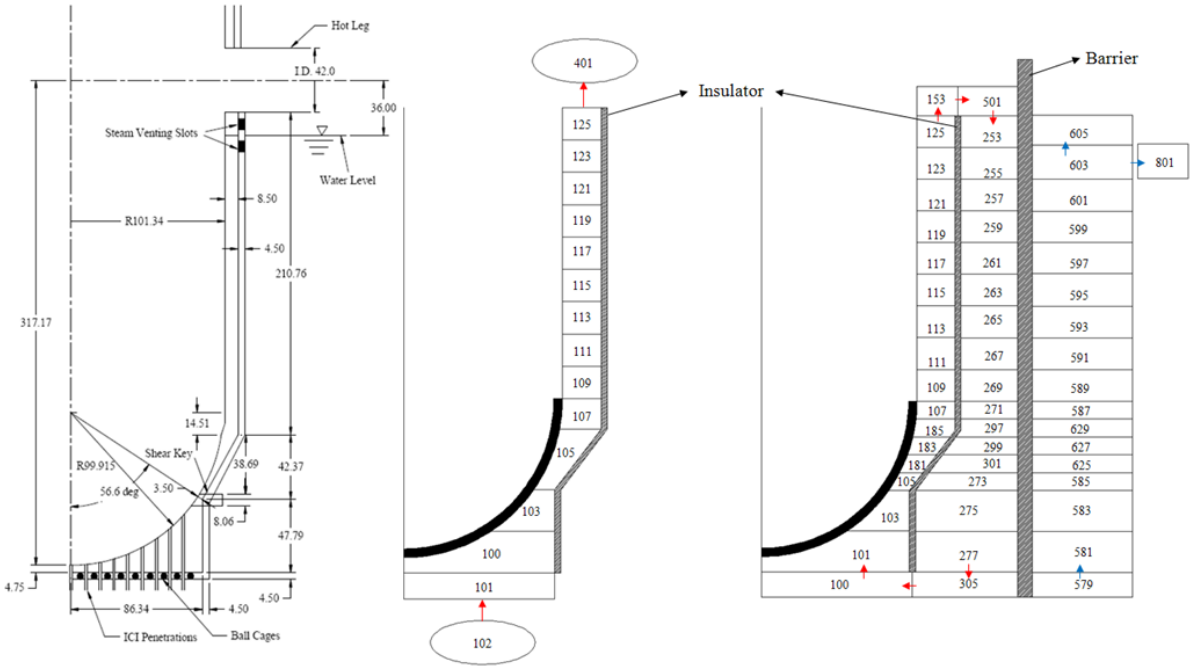

(a) (b) (c)

Fig. 4-2 Geometry comparison of (a) schematic of APR 1400 reactor vessel and insulator (Unit : inch)[40]; (b) nodalization of the existing IVR-ERVCS, and (c) nodalization of the current IVR-ERVCS

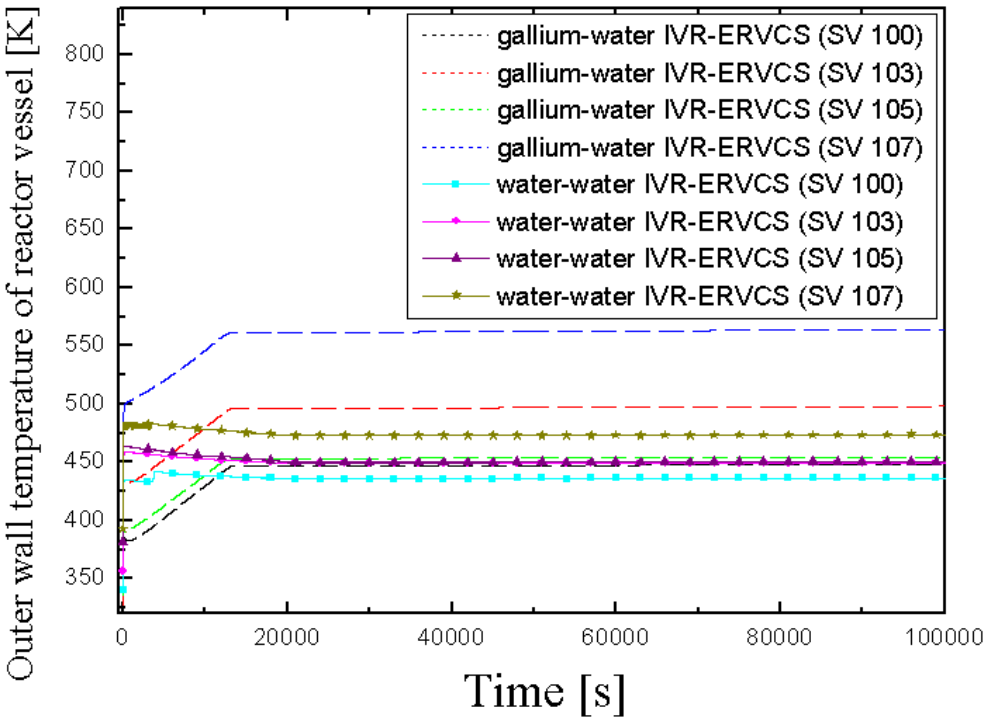

Fig. 4-3 Wall temperature distribution of outer reactor vessel of the gallium-water and water-water IVR-ERVCS under MBLOCA

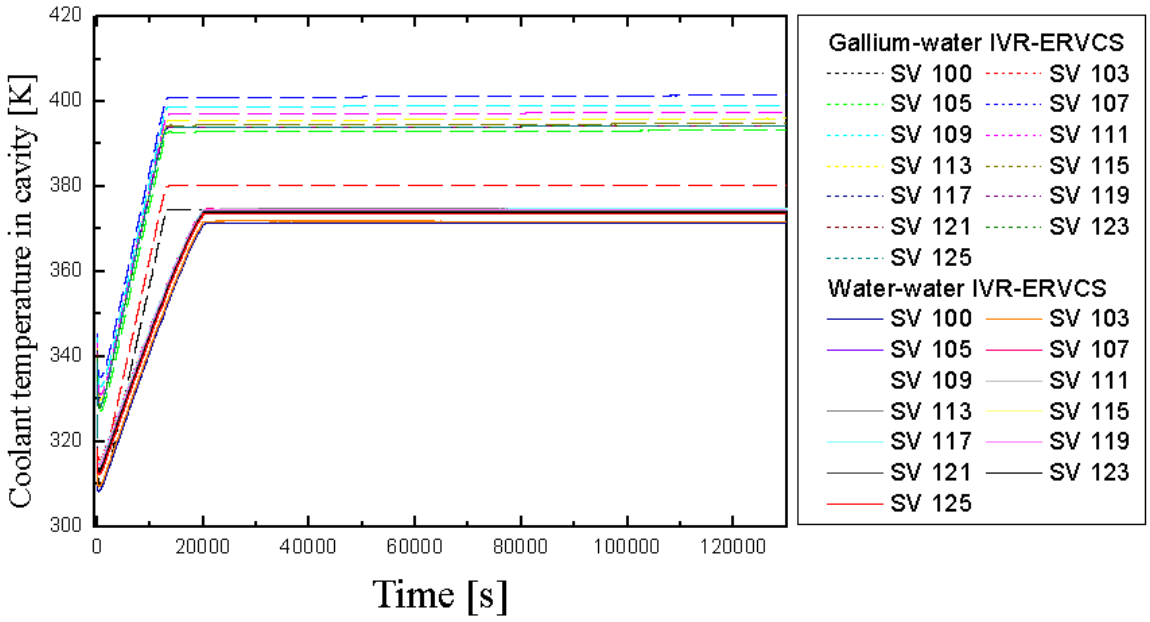

Fig. 4-4 Coolant temperature distribution in the cavity of the liquid gallium for gallium-water IVR-ERVCS and water for water-water IVR-ERVCS under MBLOCA

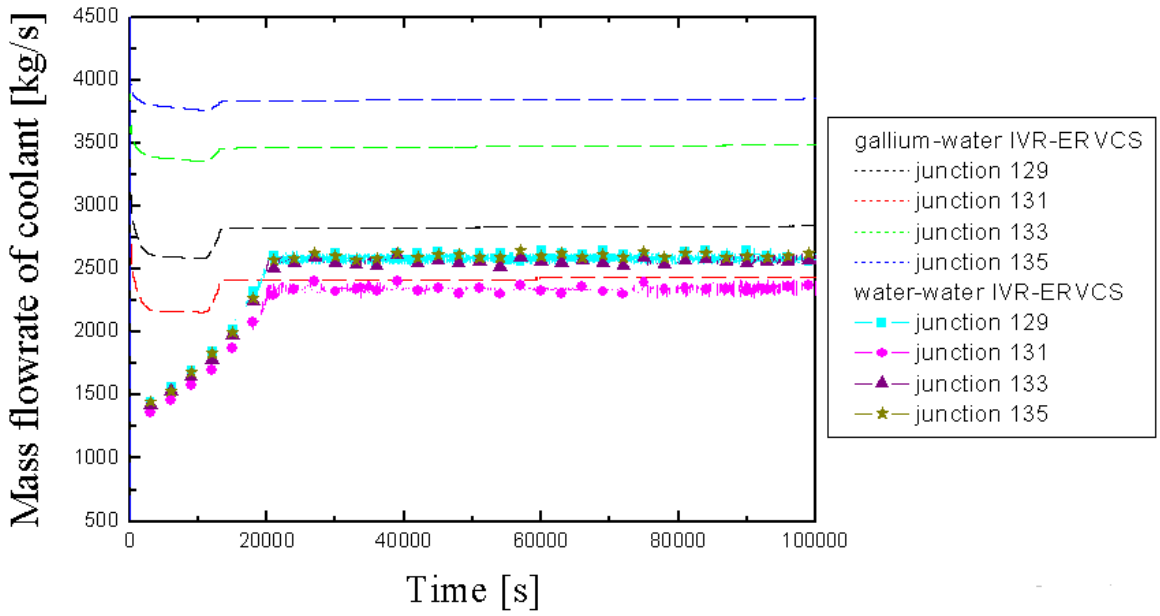

Fig. 4-5 Mass flow rate of the liquid gallium of the gallium-water IVR-ERVCS and water of the water-water IVR-ERVCS

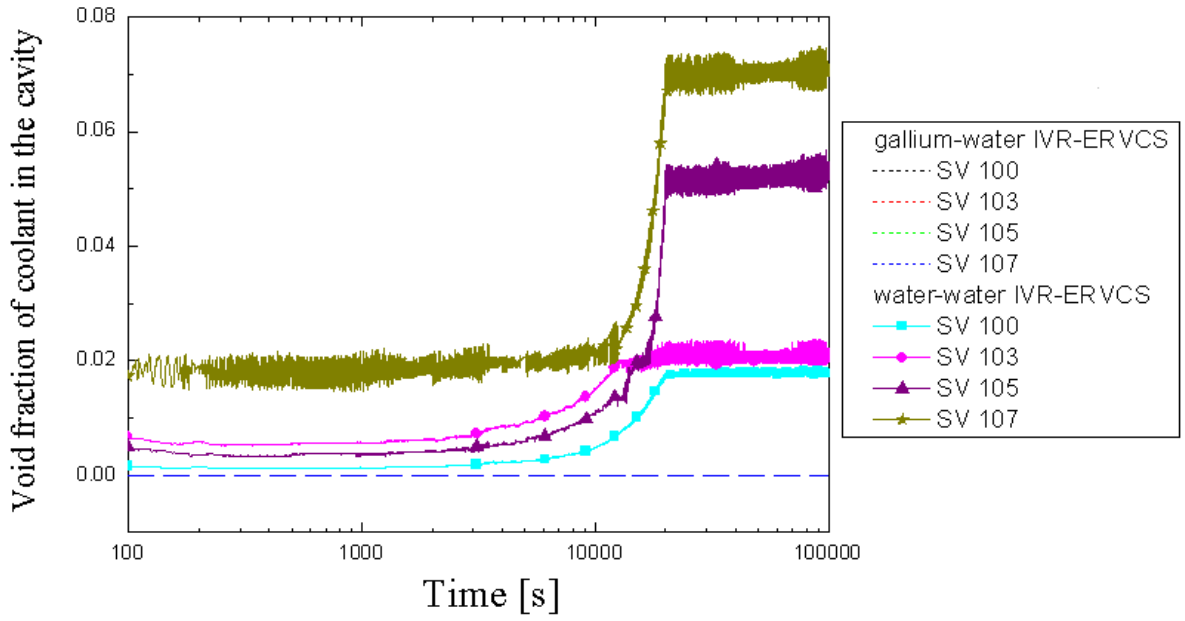

Fig. 4-6 Void fraction of gallium and water as a coolant in the cavity of the gallium-water and water-water IVR-ERVCS under MBLOCA

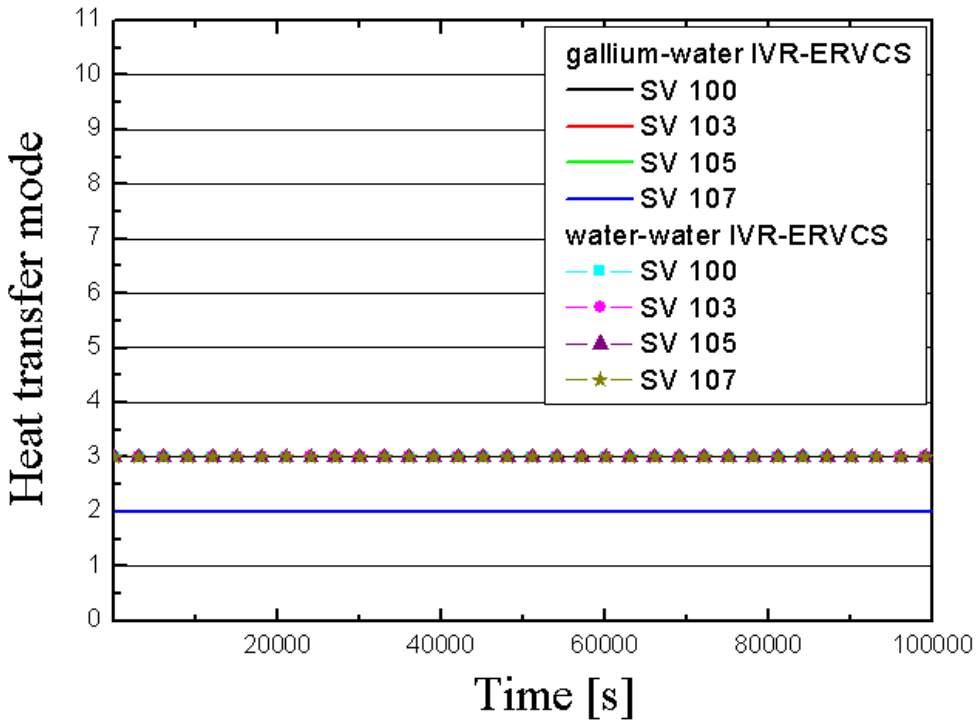

Fig. 4-7 Heat transfer mode of the gallium-water and water-water IVR-ERVCS under MBLOCA

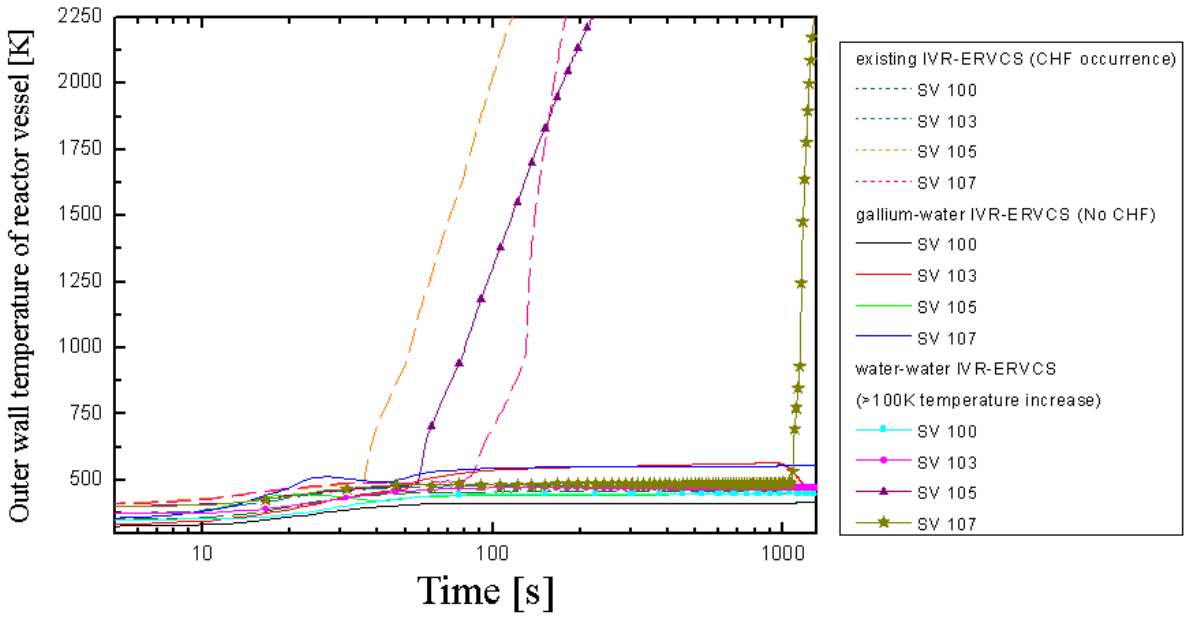

Fig. 4-8 Wall temperature distribution of outer reactor vessel of the existing, gallium-water and water-water IVR-ERVCS under LBLOCA

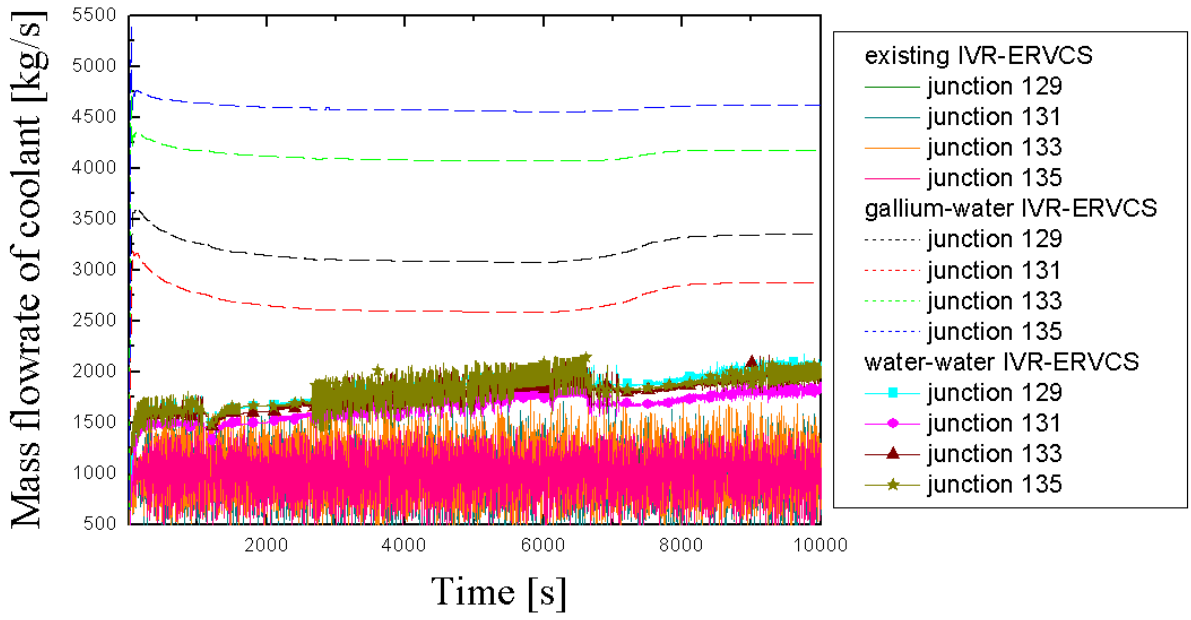

Fig. 4-9 Mass flow rate of water of the existing IVR-ERVCS, liquid gallium of the gallium-water IVR-ERVCS, and water of the water-water IVR-ERVCS

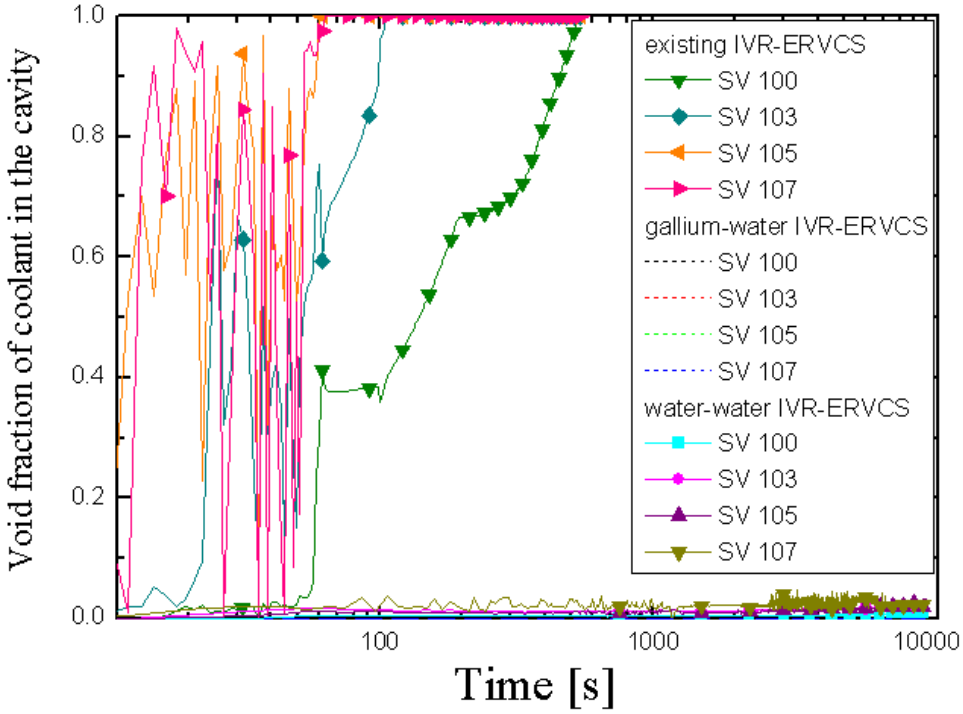

Fig. 4-10 Void fraction of a coolant in the cavity of the existing, gallium-water and water-water IVR-ERVCS under LBLOCA

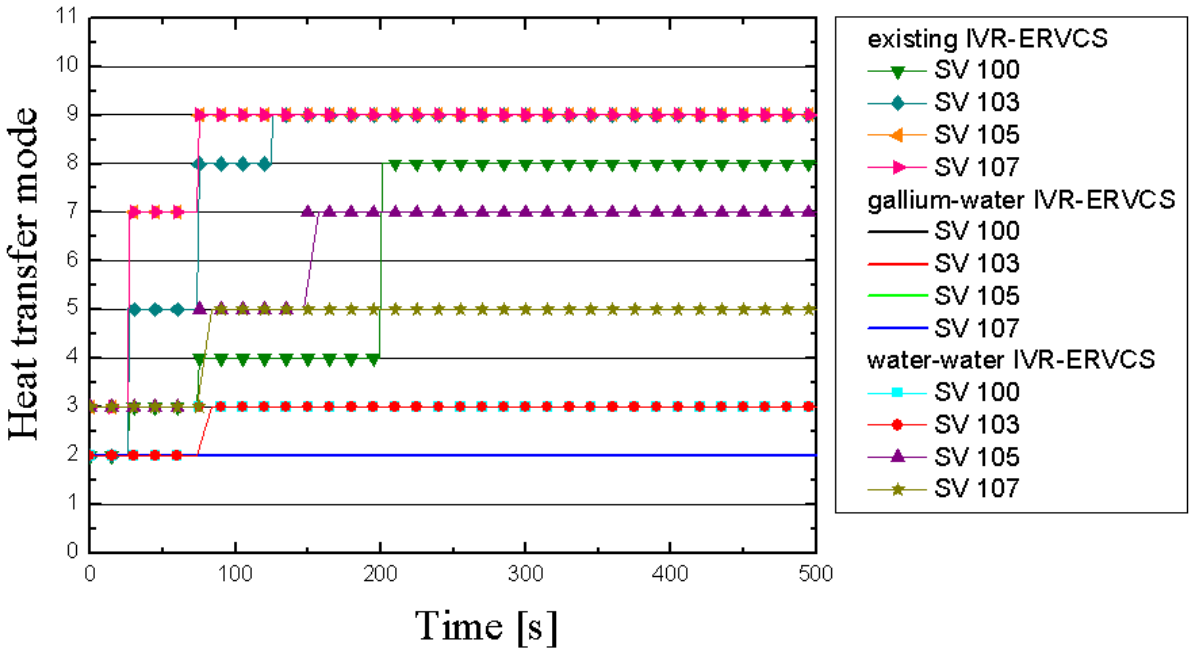

Fig. 4-11 Heat transfer mode of the existing, gallium-water and water-water IVR-ERVCS under LBLOCA

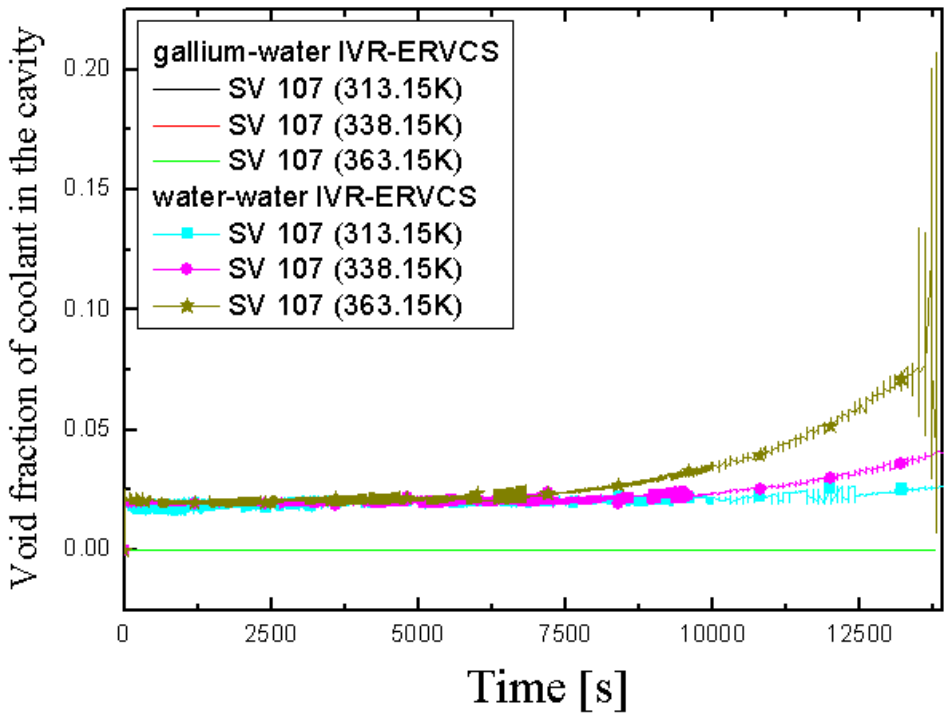

Fig. 4-12 Void fraction according to the initial temperature of the gallium-water and water-water IVR-ERVCS

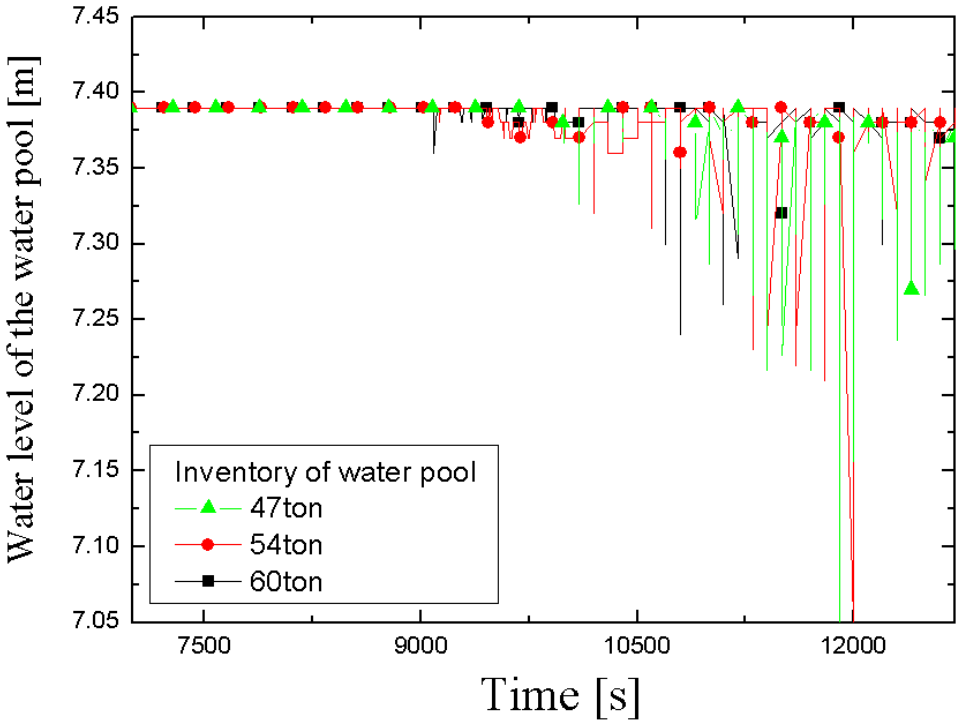

Fig. 4-13 Comparison of the water level of the water pool as an ultimate heat sink having different inventory

Chapter 5. Numerical study of liquid gallium cooled passive decay heat removal systems

5.1 Introduction

The concept of an ultra long-cycle fast reactor was introduced in the 1950s, and recently it is being actively investigated as a means to improve uranium utilization and solve the nuclear proliferation including cost reductions, low proliferation risk, and the interim storage of spent fuel. Also, this reactor type has been developed in UNIST, Ultra long-life-core fast reactor – 100 (UCFR-100). UCFR-100 is a 260 MW_{th} / 100 MW_e sodium-cooled fast reactor which requires no on-site refueling and meets the needs for future nuclear energy systems.

The safety issues of the liquid metal-cooled fast breeder reactors such as sodium-cooled fast reactors (SFRs) are important due to the fact that it uses sodium as a nuclear coolant, reacting vigorously with water and air. For that reason, there are efforts to seek for alternative candidates of liquid metal coolants having excellent heat transfer property and to adopt improved safety features to the SFRs concepts.

This part considers gallium as alternative liquid metal coolant applicable to safety features in terms of chemical activity issue of the sodium. As the liquid metal coolant, liquid gallium has technical advantages such as the low melting point in the atmospheric pressure, the high boiling point, the low pressure of saturated vapor, a relatively low coefficient of volumetric thermal expansion, a chemical reaction safety, low oxygen reactivity and a low toxicity of saturated vapor. The negative reactivity feedback induced by a relatively low thermal expansion of liquid gallium ensures the inherent safety of the core.

However, it is excluded to consider gallium as a primary coolant of the reactor since gallium has a higher macroscopic absorption cross section than other liquid metals that adversely affects neutron economy.

Therefore, the attractive properties ensure that gallium can play an important role in nuclear safety as an alternative coolant of the passive decay heat removal systems (PDHRS) of UCFR-100. Because gallium has the chemical reaction safety compared to sodium, it can be used as a boundary material between sodium and atmosphere to enhance the nuclear safety of UCFR-100.

In this part, design studied for neutronics and thermal-hydraulics are included. The safety performance of UCFR-100 was analyzed with MARS-Ga which is applicable for gallium-cooled systems.

5.2 Literature survey

Table 5-1 indicates the representative design of ultra long-cycle fast reactors in the worldwide. CANDLE[46-70] (Constant axial shape of neutron flux, nuclide densities and power shape during life of energy production) is one of the thoroughly studied by Sekimoto et al. CANDLE burn-concept has been applied to many reactor types, such as LBE cooled fast reactor, high temperature gas cooled reactor (HTGR), small long life fast reactor, supercritical water cooled fast reactor, and SFRs[70]. Compared to other ultra long-cycle fast reactors, CANDLE has the various designs having the wide range of the capacity and coolants such as helium, LBE, sodium, and lead. Among the several reactor types, safety analysis for small long life fast CANDLE reactor was performed with ULOF (unprotected loss of flow), SDRW (unprotected shut down rods withdrawal), ULOHS (unprotected loss of heat sink), and LB (local blockage) accidents in 2008[57]. In ULOF accident, the temperatures of core materials after convergence were higher than those of normal operation state. The reactivity from radial expansion gave largest negative contribution, while the Doppler effect turns positive because of the temperature drop in cool pool. In this accident, the natural convection plays the important role and protects the reactor. In SDRW accident, it showed that the core still can stay safe with large temperature margins to the limits. The hot and cold pools were the keys to keep the system safety as they were the only heat absorbers except the core itself. In ULOHS accident, the Doppler effect was most dominant and negative feedback and it comes from the large temperature increase in fresh fuel region of core, where the U238 is much abundant. The local blockage accident would not bring noticeable influence to the whole core. The results of safety analysis showed that the small long life CANDLE fast reactor has excellent inherent safety features.

TWR[70-74] (Traveling-wave reactor) has been developed by TerraPower, LLC. Due to the engagement of Bill Gates and his funded company TerraPower, TWR has been receiving more attention[70]. The transient analyses of TWR-P reactor as one of the design of TWRs were performed using SAS4A/SASSYS1 safety code[74] in 2013. The major categories of anticipated transient without scram (ATWS) included loss of flow without scram (LOFWS), loss of heat sink without scram (LOHWS) and reactivity insertion without scram (RIWS). In LOFWS, the only component of reactivity predicted to be positive is the coolant void, and the dominant source of negative reactivity feedback is the core radial expansion. In addition to LOFWS, LOHWS and RIWS accidents were also analyzed showing even smaller peak fuel and cladding temperature than LOFWS. Overall, safety analyses using SAS4A/SASSYS1 code showed that TWR-P has desirable safety characteristics. This included no sodium boiling in ATWS due to the inherent reactivity feedback. TerraPower is committed to maturing TWR technology in order to enable near-term deployment by the early 2020s.

SSTAR[75-79] (Small secure transportable autonomous reactor) is a US project for the design of a very

small modular reactor. The construction method is innovative because the site receives the completed modules, ready to be assembled. SSTAR has a pool layout cooled by natural convection of pure lead and nitride fuel, requiring a pyro-process to close the fuel cycle. SSTAR allows the adoption of S-CO_2 Brayton cycle which is more compact than a conventional solution. A prototype design, called SUPERSTAR (Sustainable proliferation-resistance enhanced refine secure transportable autonomous reactor) has been proposed for surpassing some technical problems which have prevented the near term deployment of SSTAR. This experimental reactor uses metal alloy fuel and subcritical steam Rankine cycle for electricity production with a lead intermediate circuit.

4S[79-83] (Super-safe, small, and simple) is a SFR designed by Toshiba with 30-year refueling. It has a pool layout reactor with a core thermal power of 30 MW_{th} that feeds a steam Rankine cycle producing 10 MW_e. Low maintenance requirements are achieved by simplifying the design and minimizing the use of active components, and by using electromagnetic pumps, without moving parts. The reactor building is located below ground level, providing substantial protection against an aircraft impact. The safety performance was analyzed with ARGO-3, which is a plant dynamics code of a SFR[81]. Some events, such as ULOF, UTOP (unprotected transient overpower) were selected as typical cases from various transients and accidents. The results of these simulation showed that 4S reactor has margin for safety acceptance criteria. Based on the design of Toshiba, the preliminary pin-cell simulation was also conducted with the Monte Carlo code, MCNP to obtain useful neutronics design information.

PASCAR[84] (Proliferation-resistant, accident-resistant, self-supported, capsular and assured reactor) is a LBE small modular reactor developed by Seoul National University. In safety analyses, two uncontrolled transient scenarios were considered such as UTOP and ULOHS (Unprotected loss of heat sink). Two accident analyses demonstrated inherent safe shutdown capability enough to guarantee safety margin for fuel melting with negative reactivity feedback and passive decay heat removal ensuring sufficient safety margin for fuel melting.

AFR-100[85-87] (Advanced fast reactor) was developed targeting a small electrical grid to be transportable to the plant site and operable for a long time without frequent refueling by Argonne National Laboratory. It confirmed that the evaluated reactivity coefficients provided sufficient negative feedbacks and the reactivity control systems provided sufficient shutdown margins in 2012.

Compared to other designs of ultra long-cycle reactors, UCFR-100 considers gallium as a liquid metal coolant in decay heat exchanger in PDHRS that may enhance the passive safety features of UCFR-100. By using gallium, UCFR-100 can operate not the air but water as an ultimate heat sink.

5.3 Steady-state of UCFR-100

UCFR-100 is a pool type reactor with metallic fuels, four intermediate heat exchangers, two steam

generators, and passive decay heat removal systems as shown in fig. 5-1. Table 5-2 shows the design parameters of UCFR-100. For the UCFR-100 design, the net plant power is 260 MW_{th} and 100 MW_e having 38.5 % efficiency. The core of UCFR-100 was designed to maintain for maximum 60 years[88-89]. The material of fuel, cladding, and coolant of the primary and intermediate heat transport systems are metallic fuel (U-5Zr), HT-9, and sodium respectively as shown in table 5-2.

Detailed thermal-hydraulic analysis and transient evaluation were performed by MARS-Ga. Nodalization of UCFR-100 is as shown in fig.5-2. The first heat transport system consists of the sodium coolant from component 161 to 270 including the inlet plenum, core, hot pool, shell side of intermediate heat exchanger, and pump. The intermediate heat transport system also consists of the sodium coolant from component 400 to 567 including the tube side of intermediate heat exchanger, shell side of steam generator, and pump. The tertiary system consists of the feedwater including the tube side of steam generator. The passive decay heat removal system consists of the liquid gallium coolant from component 700 to 735 including the tube side of decay heat exchanger, tube side of air heat exchanger, and expansion tank. As the ultimate heat sink, from component 910 to 935 consist of the air.

From fig. 5-3 to fig. 5-5 show the steady state condition of the primary heat transport system of UCFR-100. Fig. 5-6 and 5-7 indicate the temperature distribution of the sodium in the intermediate heat exchanger and the feedwater in the steam generator respectively. Finally, fig. 5-8 shows the liquid gallium temperature distribution in the decay heat exchanger at steady-state condition of UCFR-100.

5.4 LOF of UCFR-100

For identification of safety characteristics, design basis event, LOF (Loss of flow) was analyzed using MARS-Ga. LOF means a loss of core cooling capability, due to a pumping failure of the primary pumps. Table 5-3 indicates the safety margin and temperature limitation of SFR90-. For the safety of the structure, the average core outlet temperature should be lower than 833 K. The maximum temperature of cladding material is 923 K because of the eutectic limit of HT-9 while the maximum fuel temperature should be lower than 1228 K for reactor safety.

In this simulation, the primary pump was tripped at 0 seconds and then a reactor scram occurred after 10 seconds because of the increase of the core outlet temperature as shown in fig. 5-9 and 5-10. The power decreased drastically due to the reactor trip signal as shown in fig. 5-9 and the fuel temperature showed the highest value as shown in fig. 5-12. Fig. 5-13 and 5-14 show the gallium mass flow rate and temperature during LOF accident. At the initial stage, the sodium of the primary and intermediate heat transport system increased because of the failure of the primary cooling capability, but decreased by acting gallium-cooled PDHRS of UCFR-100. After 30 minutes, gallium-

cooled PDHRS worked, and finally the entire system of UCFR-100 became stable. Table 5-4 indicates the temperature and mass flow rate of working fluid during LOF accident and through this analysis, it confirmed that gallium can work properly as a coolant to remove the decay heat under LOF accident.

5.5 Conclusion

UCFR-100 is a 260MW_{th} / 100MW_e sodium-cooled fast reactor which requires no on-site refueling. UCFR-100 is a pool type reactor including the metallic fuels, intermediate heat exchangers, steam generators, and gallium-cooled PDHRS unlike the existing designs of sodium fast reactors. The safety analysis was performed for loss of flow (LOF) due to the pumping failure of primary pumps using MARS-Ga code. As a result, it confirmed that the liquid gallium can work properly as a boundary material between sodium and atmosphere for steady state and transient situation in UCFR-100.

Table 5-1. The representative designs of UCFR in the worldwide

Design	Country	Capacity	Years	Coolant	DHRS
CANDLE	Japan	125 MW_{th} – 3000 MW_{th}	~500	He, LBE, Na, Pb	RVACS
TWR	USA	1200 MW_{th} (500 MW_e)	40	Na	D.G. RVACS
SSTAR	USA	45 MW_{th} (20 MW_e)	30	Pb	-
4S	Japan	30 MW_{th} (10 MW_e)	30	Na	RVACS
PASCAR	Korea (SNU)	100 MW_{th} (35 MW_e)	20	LBE	RVACS
AFR	USA	250 MW_{th} (100 MW_e)	30	Na	DRACS
UCFR	Korea (UNIST)	260 MW_{th} (100 MW_e)	30 - 60	Na	PDHRS

Table 5-2. Design parameters of UCFR-100

Design parameters	Value
Net plant power [MW_{th} / MW_e]	260 / 100
Net plant efficiency [%]	38.5
Core lifetime [years]	30 – 60
Fuel	Metallic fuel (U-5Zr)
Cladding	HT-9
Primary coolant	Na
Decay heat removal system	Gallium-cooled PDHRS

Table 5-3. The safety margin and temperature limitation of SFR

Safety margin / Event category	Safety of structure		Safety of cladding		Safety of fuel	Limit of sodium boiling
	$T_{core,out}$ [K]		$T_{peak\ cladding}$ [K]		$T_{peak\ fuel}$ [K]	$T_{max\ coolant}$ [K]
	Limit	Time [hr]	Limit	Time [hr]		
Moderate frequency event	833	≤ 40,000	923	≤ 52,000	1228	1213
Infrequent event	873	≤ 1,000	943	≤ 240		
Unlikely event	923	≤ 30	973	≤ 1.2		
Extremely unlikely event	973 1033	≤ 5 ≤ 1	1063	≤ 0.3	1343	

Table 5-4. The temperature and mass flow rate of working fluid during LOF accident

Design parameters		Value	Limit
Sodium	Primary system	~ 927 K	< 1,213 K
	Intermediate system	~ 838 K	
The temperature of liquid gallium		~ 745 K	< 2,477 K
Mass flowrate of liquid gallium		137.5 kg/s	-

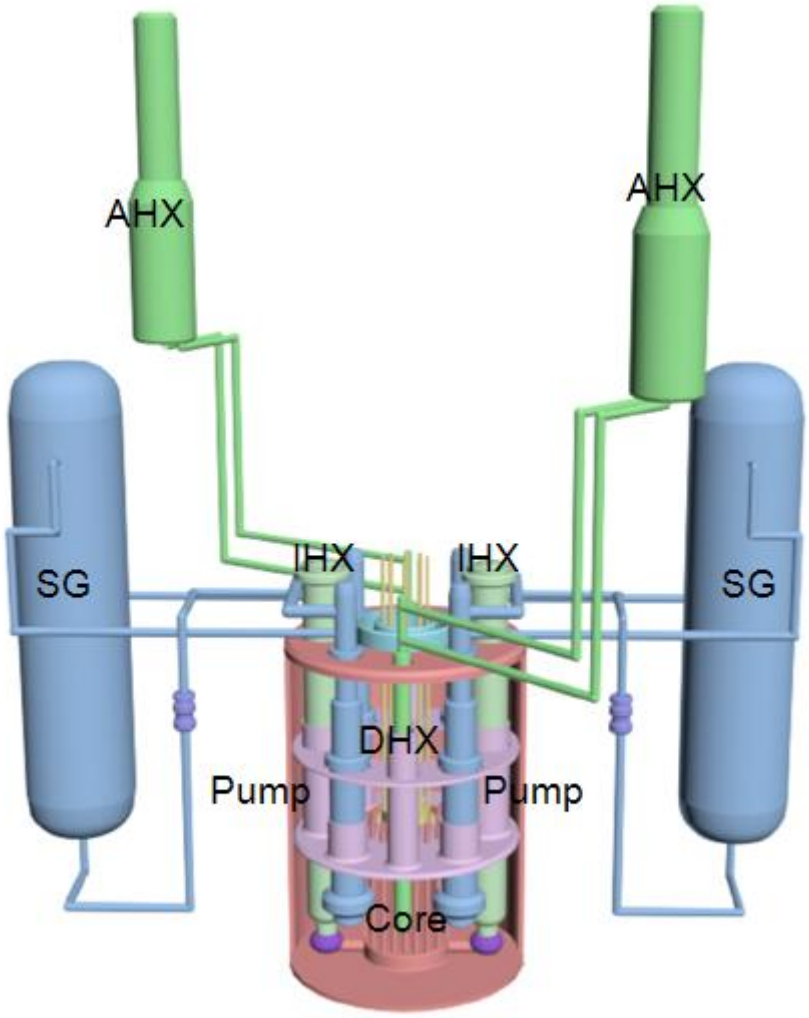

Fig. 5-1 Schematic of UCFR-100

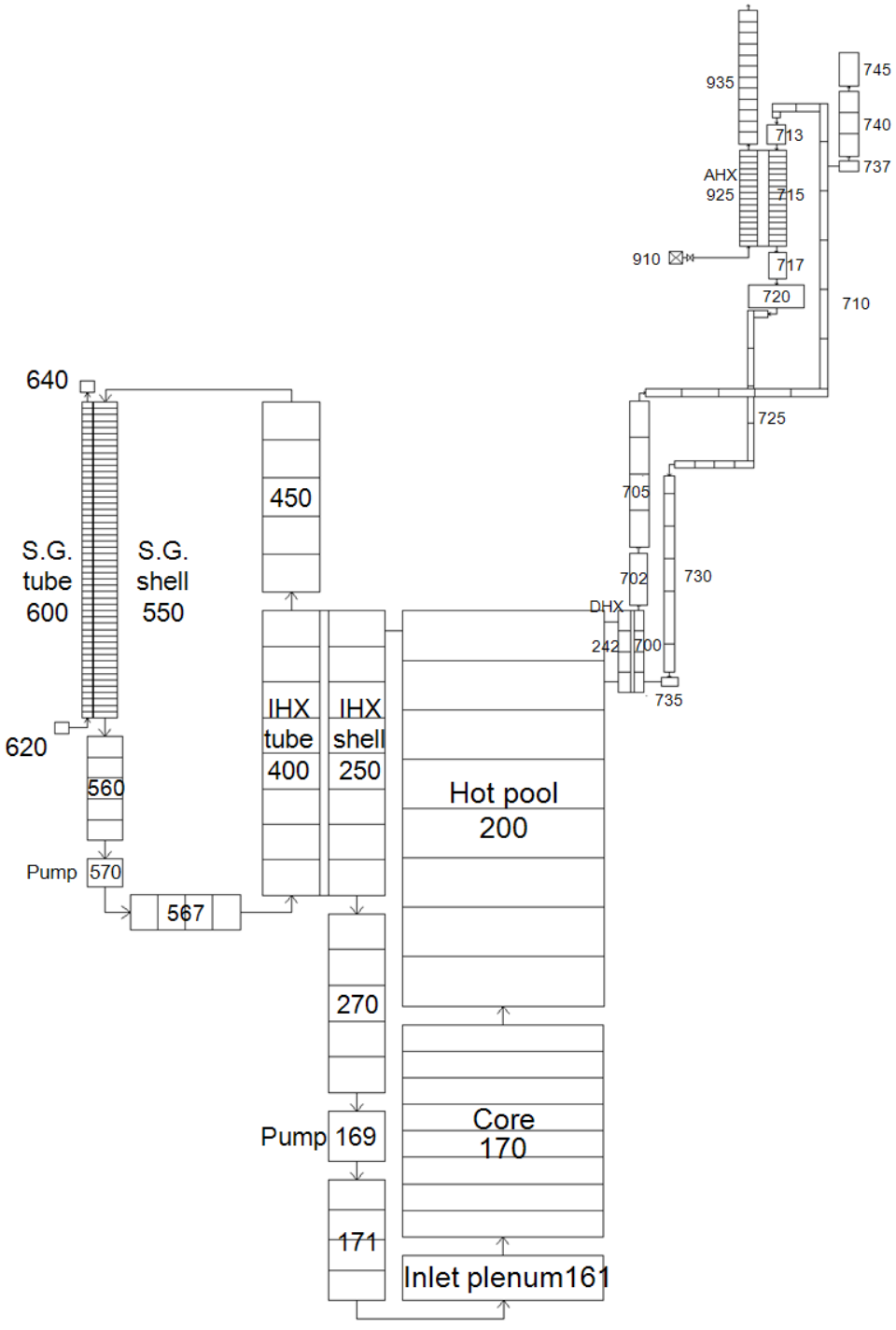

Fig. 5-2 Nodalization of UCFR-100

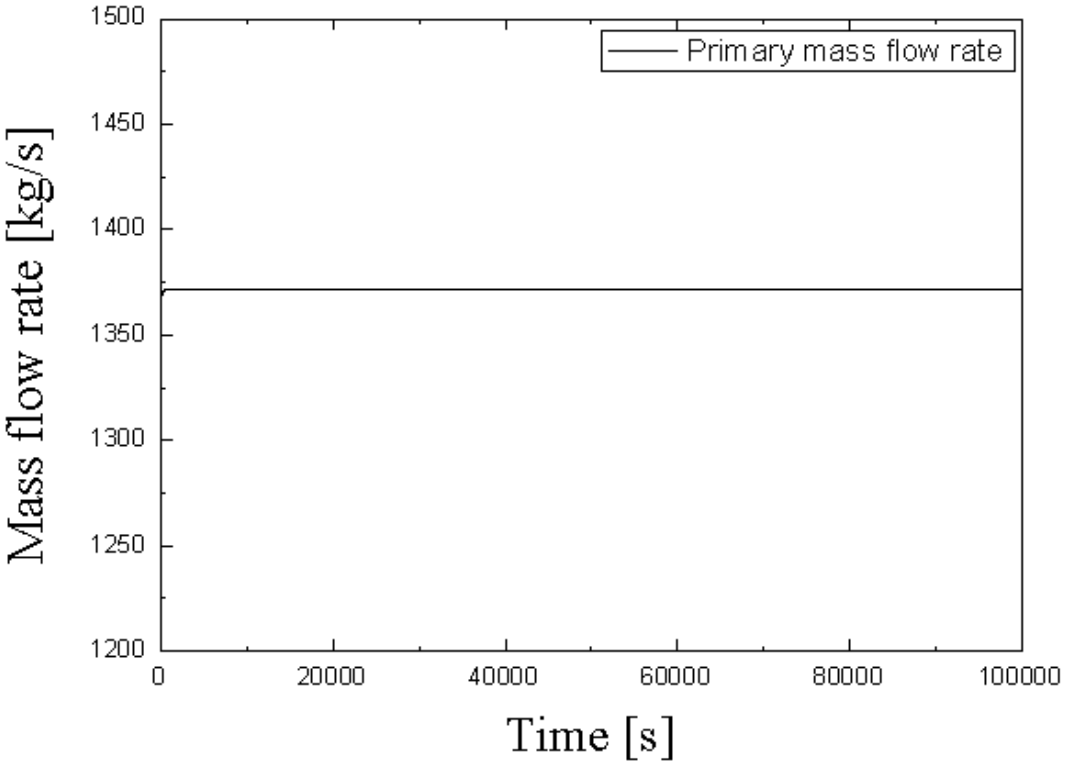

Fig. 5-3 Primary mass flow rate of UCFR-100

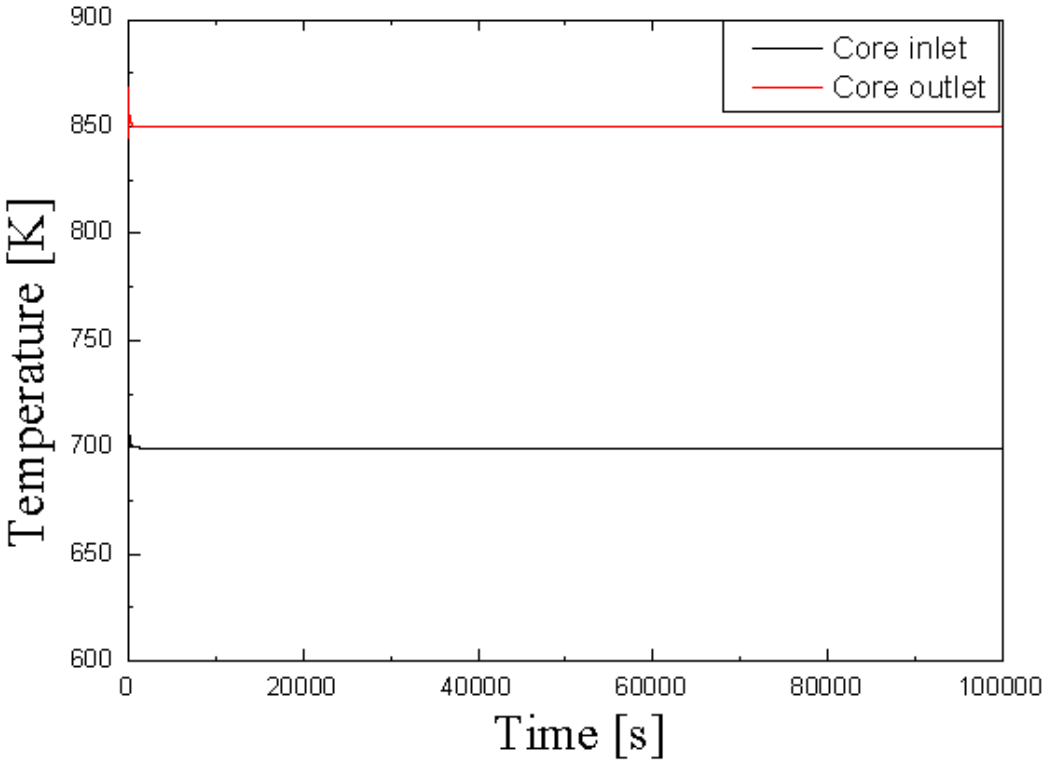

Fig. 5-4 Core inlet and outlet temperature distribution of UCFR-100

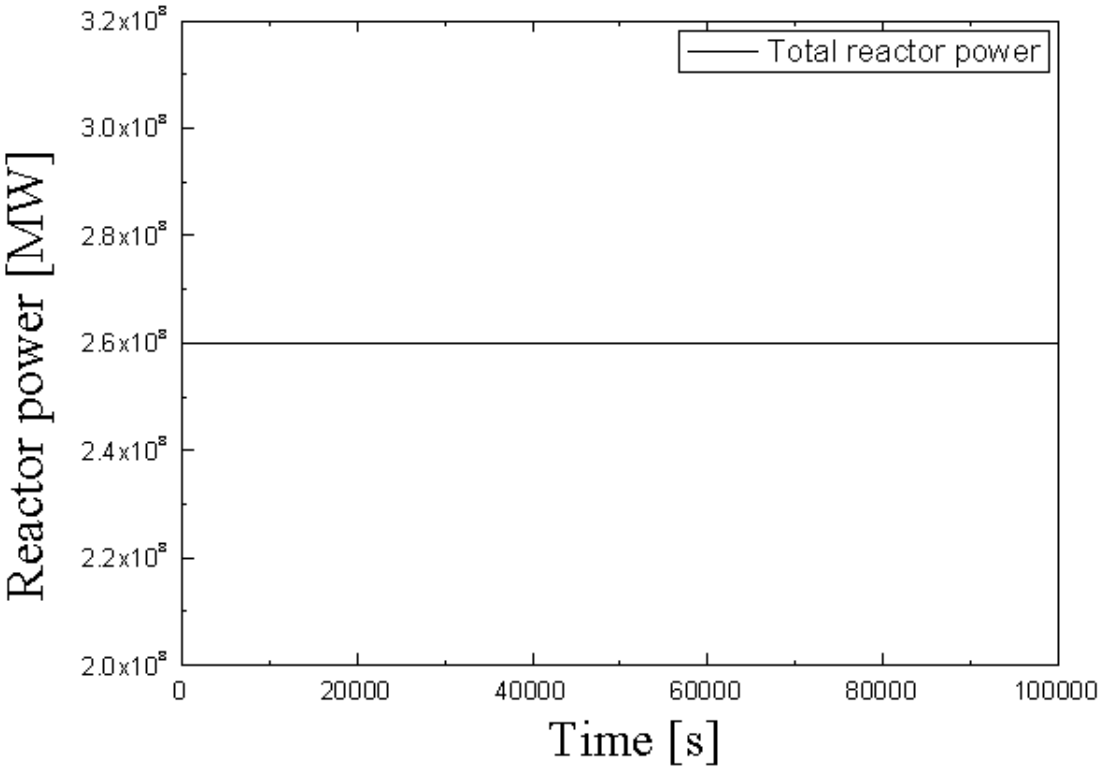

Fig. 5-5 Reactor thermal power of UCFR-100

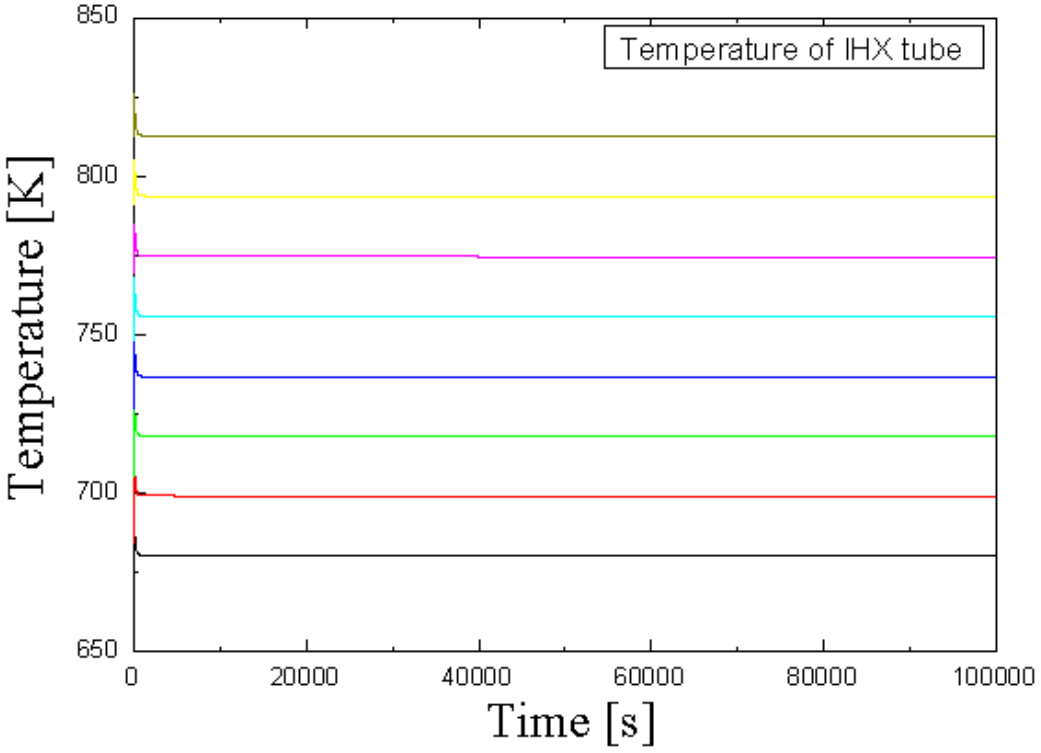

Fig. 5-6 Tube side - temperature distribution in the intermediate heat exchanger of UCFR-100

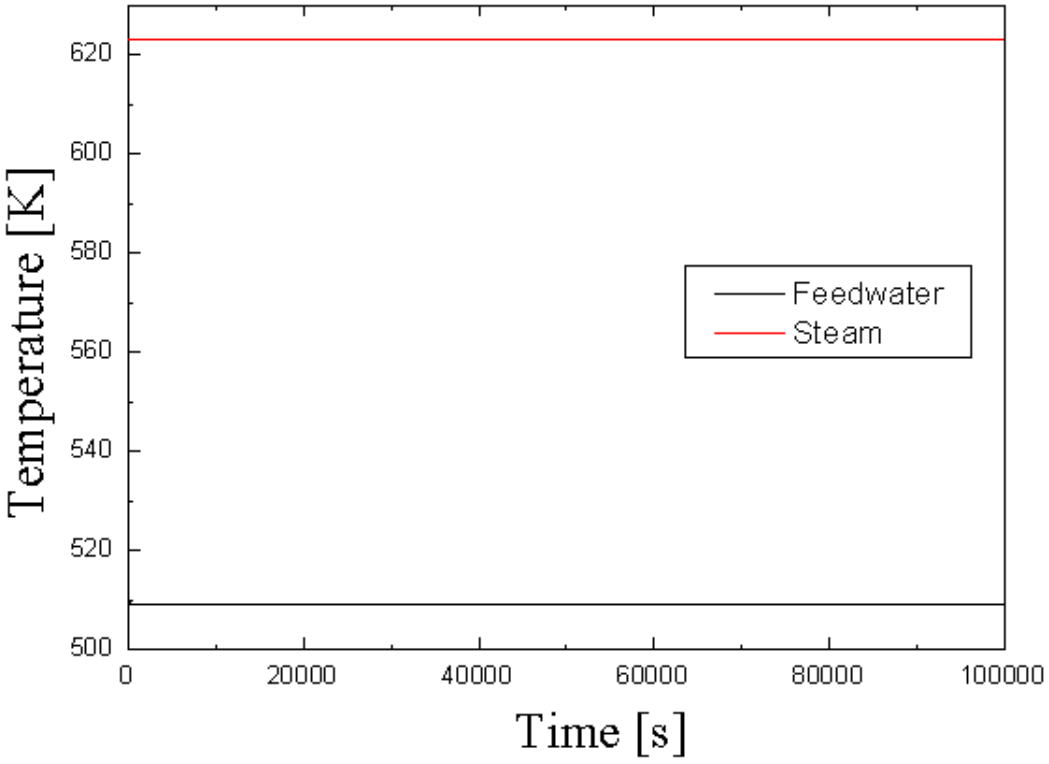

Fig. 5-7. Feedwater and steam temperature distribution of UCFR-100

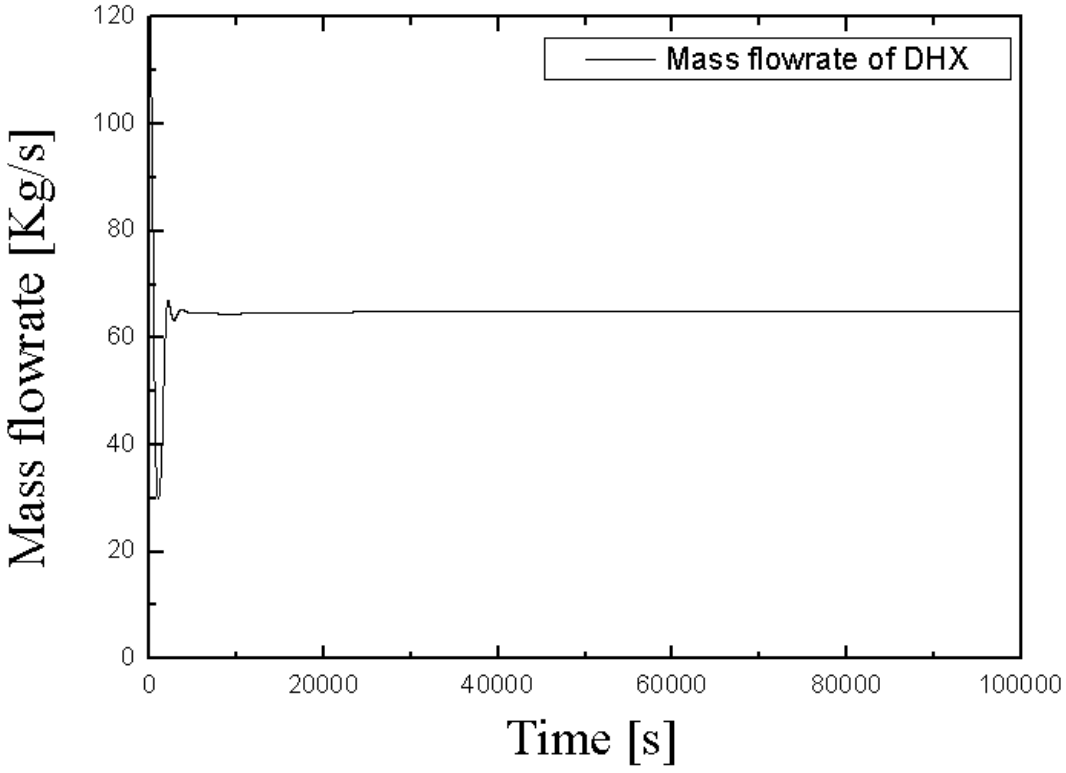

Fig. 5-8. Gallium temperature distribution in the decay heat exchanger of UCFR-100

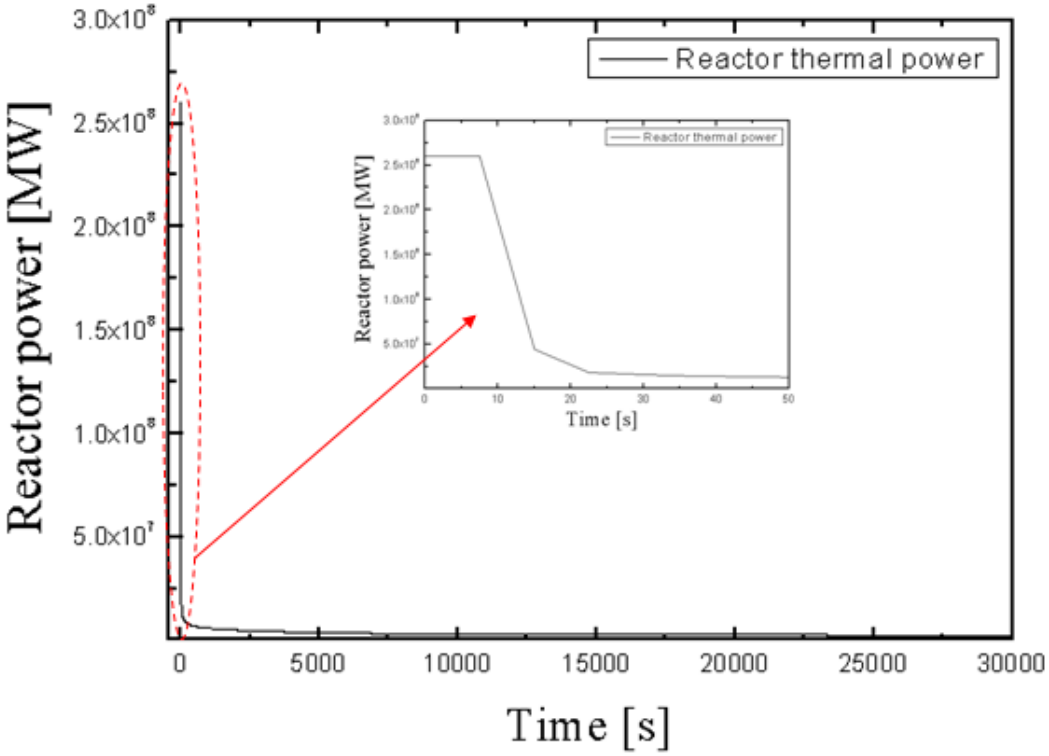

Fig. 5-9 Reactor thermal power during LOF accident

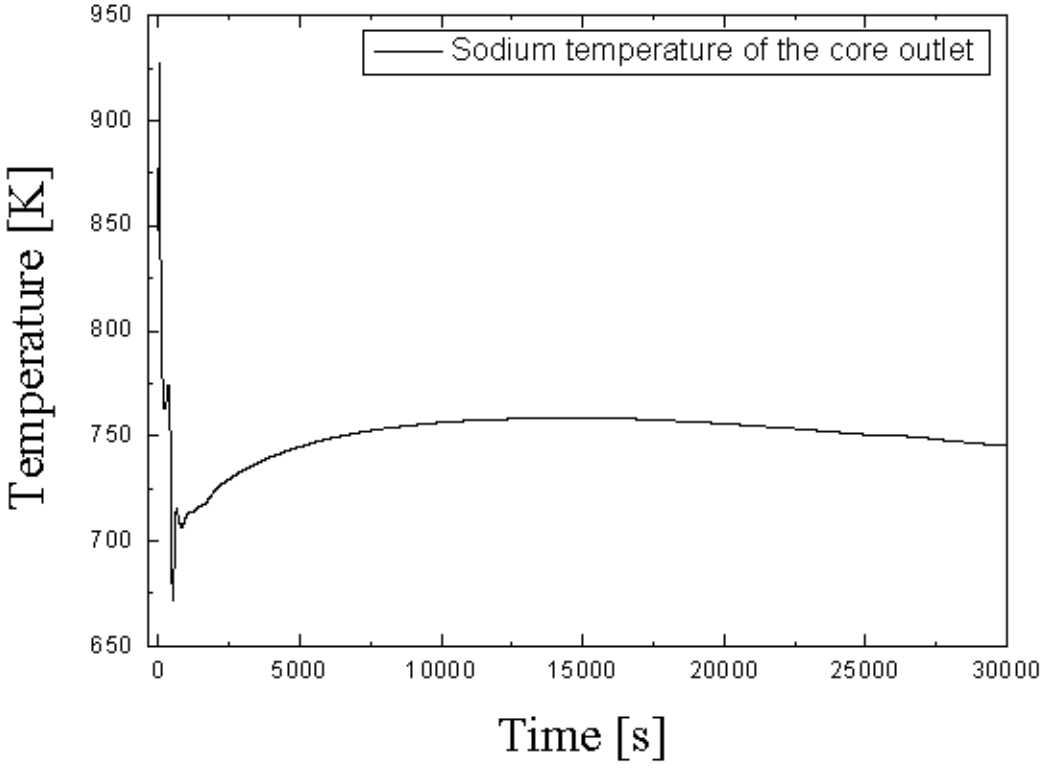

Fig, 5-10 Sodium temperature of the primary heat transport system in UCFR-100

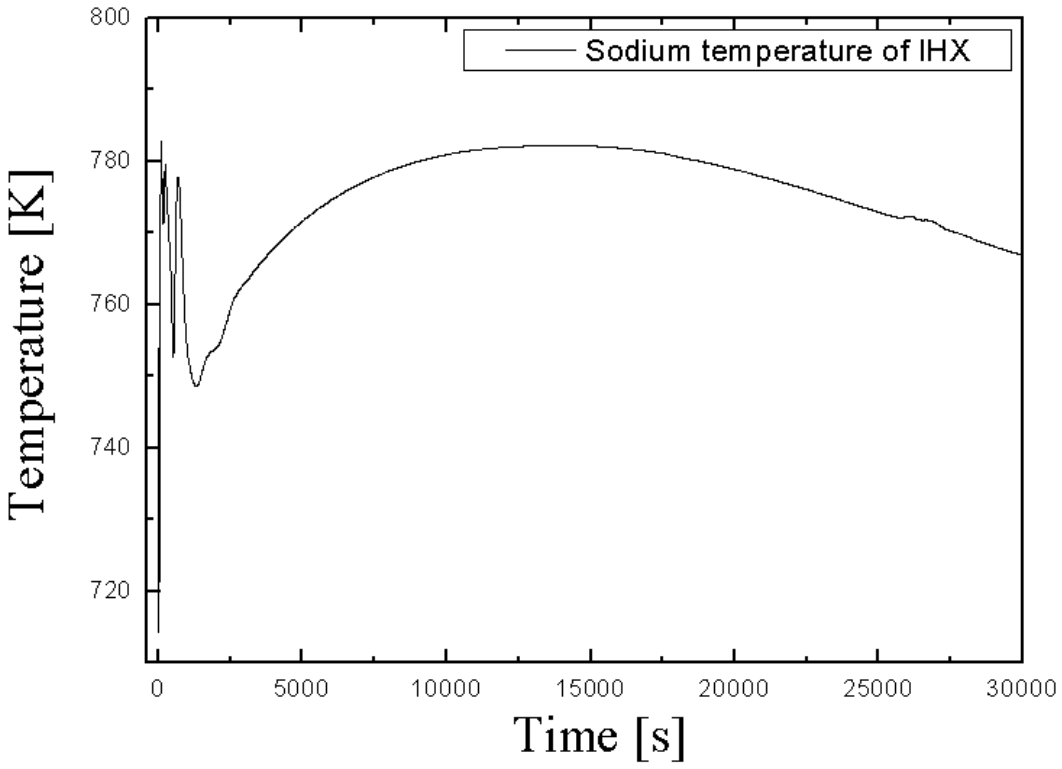

Fig. 5-11 Sodium temperature of the intermediate heat transport system in UCFR-100

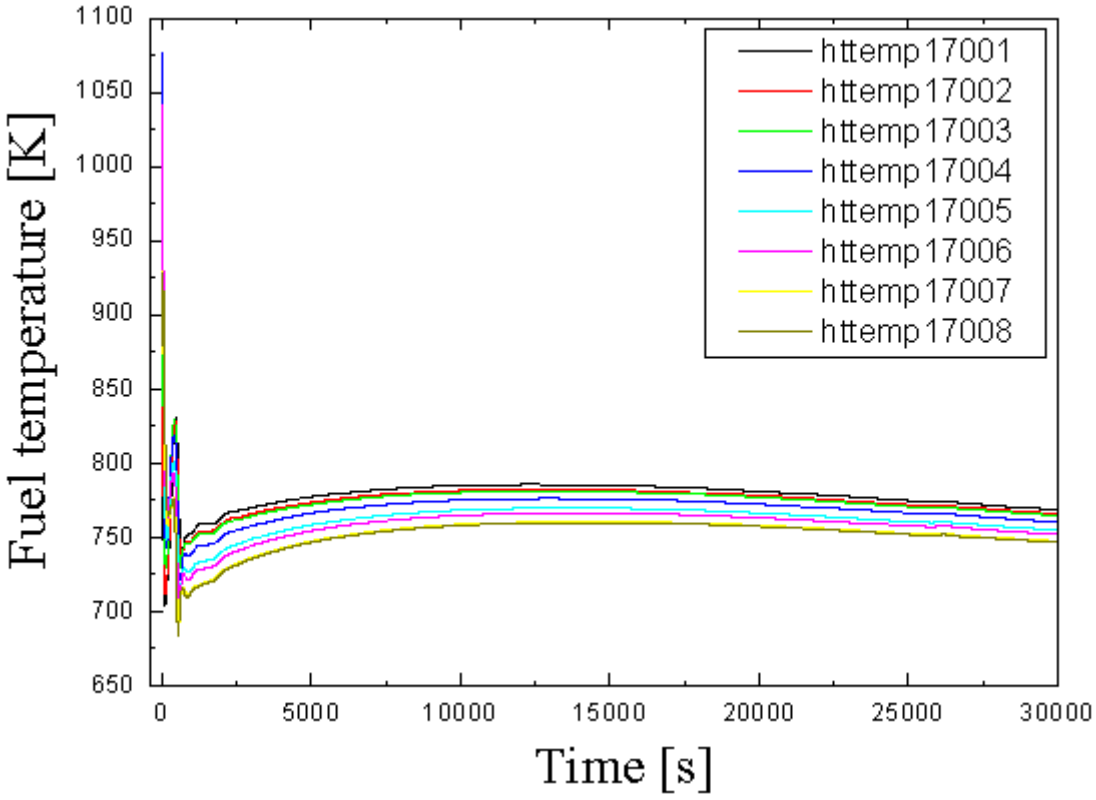

Fig. 5-12 Fuel temperature during LOF accident

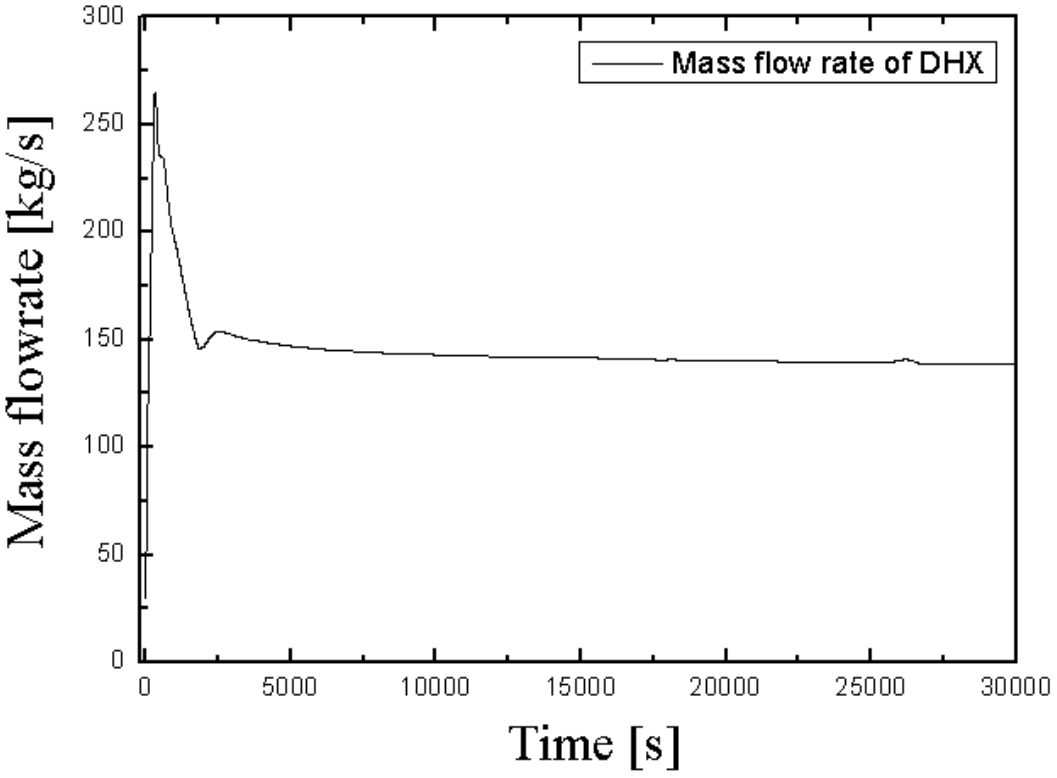

Fig. 5-13 Gallium mass flow rate of the decay heat exchanger during LOF accident

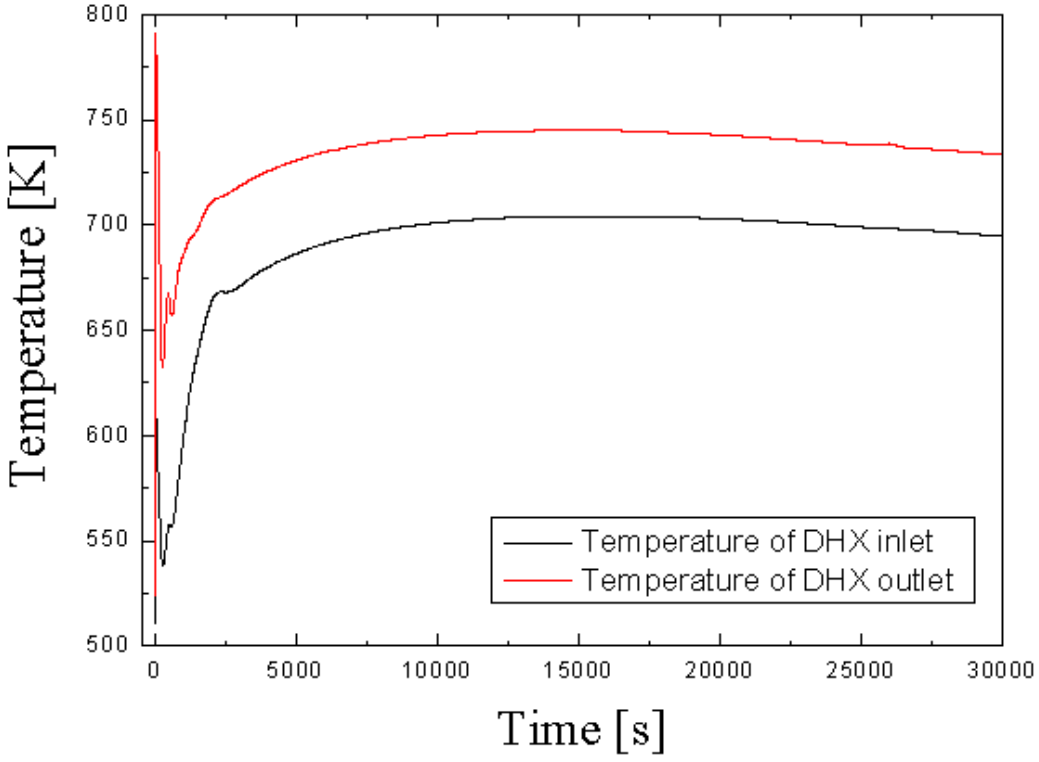

Fig. 5-14 Gallium temperature of the decay heat exchanger during LOF accident

Chapter 6. Conclusions and recommendations

6.1 Conclusions

6.1.1 Experimental study of natural convection heat transfer using gallium properties

The study on natural convection capability of gallium was carried out in a rectangular loop consisted of stainless steel 316L tube. During the experimental process, steady state natural convection for gallium observed within the heat flux range of 6.17×10^3 to 5.07×10^4 W/m^2. From the experimental observations, mass flow rate of liquid gallium was obtained by measuring the differential pressure of liquid gallium using orifice and dp transmitter and heat average heat transfer coefficients can be calculated by measuring the surface temperature of the flow path and the temperature of liquid gallium from thermocouples. The experimental data of average Nusselt numbers are 3 and 4 times lower than the values given by Schulenberg[21] and Sugiyama[22] et al. respectively.

A numerical code, MARS-Ga was developed to predict the behavior of gallium in the loop and was validated against the experimental results. It was found that the predictions are in good agreements of the trend with the experimental results as well as CFD analysis.

6.1.2 Numerical study of liquid gallium cooled passive decay heat removal systems

In the numerical analyses, the evaluations of the gallium-water in-vessel corium retention through external reactor vessel cooling system (IVR-ERVCS) in APR 1400 and gallium-cooled passive decay heat removal system (PDHRS) in UCFR-100 were performed using MARS-Ga code. The attractive properties such as the low melting point, the high boiling point, and no reaction with water ensure that gallium can play an important role in nuclear safety as an alternative coolant in PWR and SFR.

Through these analyses, it confirmed that the liquid gallium can work properly as a boundary material between sodium and atmosphere for steady state and transient situation in UCFR-100.

6.2 Recommendations

In this study, the gallium was suggested as a coolant in a cavity of APR 1400 and PDHRS of UCFR-100. Also, the feasibility of the gallium-water IVR-ERVCS and PDHRS of UCFR-100 was confirmed through this study using MARS-Ga. To solve the limitation of the existing systems and to ensure the sufficient thermal margin, gallium-cooled passive decay heat removal systems can be a successful strategy for mitigating severe accidents in PWRs such as APR 1400 or higher power-

capacity nuclear power plants. Also, it can work as a boundary material between sodium and atmosphere for steady state and transient situation in Gen IV reactors such as SFRs.

References

1. Fanning T.H.; Sodium as a fast reactor, U.S. Nuclear regulatory commission, U.S.A., **2007**.
2. Silverman I.; Yarin A.L.; Reznik S.N.; Arenshtan A.; Kijet D.; Nagler, A.; High heat-flux accelerator targets: Cooling with liquid metal jet impingement. *International Journal of Heat and Mass Transfer*, **2006**, 49, 2782-2792.
3. Sawada T.; Netchaev A.; Ninokata H.; Endo H.; Gallium-cooled liquid metallic-fueled fast reactor. *Progress in Nuclear Energy*, **2000**, 37, 313-319.
4. Yamanaka Y.; Kakimoto K.; Ozoe H.; Churchill S.W.; Rayleigh-Bernard oscillatory natural convection of liquid gallium heated from below. *Chemical Engineering Journal*, **1998**, 71, 201-205.
5. Stankus S.V.; Khairulin R.A.; Mozgovoy A.G.; Roshchupkin V.V.; Pokrasin M.A.; The density and thermal expansion of eutectic alloys of lead with bismuth and lithium in condensed state. *Journal of Physics : Conference Series*, **2008**, 98.
6. Pashaev B.P.; Palchaev D.K.; Paschuk E.G.; Density, ultrasound speed, electrical and thermal conductivity of fusible metals in liquid state/reviews on thermo physical properties of materials. *Russia: M.*, **1982**
7. Tolli J.; Overview of property formulations for helium, nitrogen, lithium, and lithium-lead in ATHENA/MOD1 with comparison of calculated properties to measured properties, BG&G Idaho Inc., **2005**
8. Young D.A.; A soft-sphere model for liquid metals, University of California, Livermore, California, **1977**
9. Blink J.A.; Lithium equation-of-state, University of California, Livermore, California, **1982**
10. Davis C.B.; Implementation of molten salt properties into RELAP5-3D/ATHENA, INEEL/EXT-05-02658, Idaho National Laboratory, January, **2005**.
11. Choi S.; Cho J.H.; Bae M.H.; Lim J.; Puspitarini D.; Jeun J.H.; Joo H.G.; Hwang I.S.; PASCAR: Long burning small modular reactor based on natural circulation. *Nuclear Engineering and Design*, **2011**, 241, 1486-1499.
12. Cengel Y.A. & Boles M.A.; Thermodynamics: An engineering approach in SI units, *McGraw-Hill companies, Inc.*, **2006**.
13. Cochran C.N. & Foster L.M.; Vapor pressure of gallium, stability of gallium suboxide vapor, and equilibria of some reactions producing gallium suboxide vapor, *Journal of the electrochemical society*, **1962**, 109, 144-148.
14. Thermalphysical properties of materials for nuclear engineering: A tutorial and collection of data, International atomic energy agency, Vienna, **2008**

15. Hata K.; Takeuchi Y.; Shiotsu M.; Sakurai A.; Natural convection heat transfer from a horizontal cylinder in liquid sodium part 1: experimental results, *Nuclear Engineering and Design*, **1999**, 193, 105-118.
16. Jackson J.D.; Turbulent mixed convection heat transfer to liquid sodium, *International Journal of Heat and Fluid flow*, **1983**, 4, 107-111.
17. Davies N.W. & Sheriff N.; An experimental investigation of natural convection heat transfer from downward-facing surfaces in sodium for fast reactor internal core catchers, *International Centre for Heat and Mass Transfer*, **1982**.
18. Borgohain A.; Jaiswal B.K.; Maheshwari N.K.; Vijayan P.K.; Saha D.; Sinha R.K.; Ntural circulation studies in a lead bismuth eutectic loop, *Progress in Nuclear Energy*, **2011**, 53, 308-319.
19. Ma W.; Karbojian A.; Sehgal B.R.; Experimental study on natural circulation and its stability in a heavy liquid metal loop, *Nuclear Engineering and Design*, **2007**, 237, 1838-1847.
20. Michiyoshi I.; Takahashi O.; Serizawa A.; Natural convection heat transfer from a horizontal cylinder to mercury under magnetic field, *International Journal Heat and Mass Transfer*, **1976**, 19, 1021-1029.
21. Schulenberg T.; Natural convection heat transfer to liquid metals below downward facing horizontal surfaces, *International Journal Heat and Mass Transfer*, **1984**, 27, 433-441.
22. Sugiyama K.; Ma Y.; Ishiguro R.; Laminar natural convection heat transfer from a horizontal circular cylinder to liquid metals, *Journal of Heat Transfer*, **1991**, 113, 91-96.
23. Hurle D.T.J.; Jakeman E.; Johnson C.P.; Convection temperature oscillations in molten gallium, *Journal of Fluid Mechanics*, **1974**, 64, 565-576.
24. Mohamad A.A. & Viskanta R.; Flow structures and heat transfer in a lid-driven cavity filled with liquid gallium and heated from below, *Experimental Thermal and Fluid Science*, **1994**, 9, 309-319.
25. Derebail R.; Koster J.N.; Numerical simulation of natural convection of gallium in a narrow gap, *International Journal of Heat and Mass Transfer*, **1997**, 40, 1169-1180.
26. Tagawa T. & Ozoe H.; Enhanced heat transfer rate measured for natural convection in liquid gallium in a cubical enclosure under a static magnetic field, *Journal of Heat Transfer*, **1998**, 20, 1027-1032.
27. Juel A.; Mullin T.; Hadid H.B.; Henry D.; Three-dimensional free convection in molten gallium, *Journal of Fluid Mechanics*, **2001**, 436, 267-281.
28. Xu B. & Li B.Q.; Hot-film measurement of temperature gradient induced natural convection in liquid gallium, *Experimental Thermal and Fluid Science*, **2005**, 29, 697-704.
29. Selver R.; Kamotani Y.; Ostrach S.; Natural convection of a liquid metal in vertical circular cylinders heated locally from the side, *Journal of Heat Transfer*, **1998**, 120, 108-114.

30. Kamotani Y.; Weng F.B.; Ostrach S.; Platt J.; Oscillatory natural convection of a liquid metal in circular cylinders, *Journal of Heat Transfer*, **1994**, 116, 627-632.
31. Todreas N.E. & Kaimi M.S.; Nuclear systems II – elements of thermal hydraulic design, *Hemisphere publishing corporation*, 1990, 67-83.
32. Vijayan P.K.; Experimental observations on the general trends of the steady state and stability behavior of single-phase natural circulation loops, *Nuclear Engineering and Design*, **2002**, 215, 139-152.
33. Kang K.H.; Park R.J.; Kim S.B.; Kim H.D.; Chang S.H.; Flow analyses using RELAP5/MOD3 code for OPR1000 under the external reactor vessel cooling, *Annals of Nuclear Energy*, **2006**, 33, 966-974.
34. Tarabelli D.; Ratel G.; Pelisson R.; Guillard G.; Barnak M.; Matejovic P.; ASTEC application to in-vessel corium intention, *Nuclear Engineering and Design*, **2009**, 239, 1345-1353.
35. Mladin M.; Dupleac D.; Prisecaru I.; Mladin D.; Adapting and applying SCDAP/RELAP5 to CANDU in-vessel retention studies, *Annals of Nuclear Energy*, **2010**, 37, 845-852.
36. Park R.J.; Lee J.R.; Ha K.S.; Kim H.Y.; Evaluation of in-vessel corium retention through external reactor vessel cooling for small integral reactor, *Nuclear Engineering and Design*, **2013**, 262, 571-578.
37. Park R.J.; Ha K.S.; Kim S.B.; Kim H.D.; Two-phase natural circulation flow of air and water in a reactor cavity model under an external vessel cooling during a severe accident, *Nuclear Engineering and Design*, **2006**, 236, 2424-2430.
38. Park S.D. & Bang I.C.; Feasibility of flooding the reactor cavity with liquid gallium coolant for IVR-ERVC strategy, *Nuclear Engineering and Design*, **2013**, 258, 13-18.
39. Park R.J.; Kim S.B.; Kim H.D.; Detailed analysis of in-vessel melt progression in the LOCA of the KSNP using the SCDAP/RELAP5, *Proceedings of the Korean Nuclear Society spring meeting*, **2004**, May 27-28, Gyeongju.
40. Kim S.B.; Kim H.D.; Koo K.M.; Park R.J.; Hong S.W.; Cho Y.R.; Kim J.T.; Ha K.S.; Kang K.H.; Kim H.Y.; Optimization of the severe accident management strategy for domestic plants and validation experiments, *Korea Atomic Energy Research Institute*, 2004, KAERI/RR-2528.
41. Churchill S.W. & Chu H.H.S.; Correlating equations for laminar and turbulent free convection from a vertical plate, *International Journal of Heat and Mass Transfer*, **1975**, 18, 1323-1329.
42. Chen J.C.; A correlation for boiling heat transfer to saturated fluids in convective flow, *Process Design and Development*, **1966**, 5, 322-327.
43. Forster H.K. & Zuber N.; Dynamics of vapor bubbles and boiling heat transfer, *AIChE Journal*, **1955**, 1, 531-535.

44. Greoneveld D.C.; Cheng S.C.; Doan T.; 1986 AECL-UO critical heat flux lookup table, *Heat transfer engineering*, **1986**, 7, 46-62.
45. Hwang J.S.; Kim J.W.; Nam H.U.; Park G.C.; Assessment of mars code for predicting critical heat flux under heaving conditions, *Nuclear Technology*, **2010**, 176, 260-273.
46. Sekimoto H.; Ryu K.; Yoshimura Y.; CANDLE: The new burnup strategy, *Nuclear Science and Engineering*, **2001**, 139, 306-317.
47. Ohoka Y. & Sekimoto H.; Application of CANDLE burnup to block-type high temperature gas cooled reactor, *Nuclear Engineering and Design*, **2004**, 229, 15-23.
48. Ohoka Y.; Watanabe T.; Sekimoto H.; Simulation study on CANDLE burnup applied to block-type high temperature gas cooled reactor, *Progress in Nuclear Energy*, **2005**, 47, 292-299.
49. Sekimoto H.; Application of CANDLE burnup strategy for future nuclear energy utilization, *Progress in Nuclear Energy*, **2005**, 47, 91-98.
50. Sekimoto H. & Udagawa Y.; Effects of fuel and coolant temperatures and neutron fluence on CANDLE burnup calculation, *Journal of Nuclear Science and Technology*, **2006**, 43, 189-197.
51. Sekimoto H. & Miyashita S.; Startup of "CANDLE" burnup in fast reactor from enriched uranium core, *Energy Conversion and Management*, **2006**, 47, 2772-2780.
52. Ismail, Ohoka Y.; Liem P.H.; Sekimoto H.; Long life small CANDLE-HTGRs with thorium, *Annals of Nuclear Energy*, **2007**, 34, 120-129.
53. Sekimoto H. & Nagata A.; "CANDLE" burnup regime after LWR regime, *Progress in Nuclear Energy*, **2008**, 50, 109-113.
54. Yan M. & Sekimoto H.; Design research of small long life CANDLE fast reactor, *Annals of Nuclear Energy*, **2008**, 35, 18-36.
55. Sekimoto H. & Yan M.; Design study on small CANDLE reactor, *Energy Conversion and Management*, **2008**, 49, 1868-1872.
56. Takaki N. & Sekimoto H.; Potential of CANDLE reactor on sustainable development and strengthened proliferation resistance, *Progress in Nuclear Energy*, **2008**, 50, 114-118.
57. Yan M. & Sekimoto H.; Safety analysis of small long life CANDLE fast reactor, *Annals of Nuclear Energy*, **2008**, 35, 813-828.
58. Liem P.H.; Ismail; Sekimoto H.; Small high temperature gas-cooled reactors with innovative nuclear burning, *Progress in Nuclear Energy*, **2008**, 50, 251-256.
59. Yan M. & Sekimoto H.; Study on small long-life LBE cooled fast reactor with CANDLE burnup – Part I: Steady state research, *Progress in Nuclear Energy*, **2008**, 50, 286-289.
60. Nagata A.; Takaki N.; Sekimoto H.; A feasible core design of lead bismuth eutectic cooled CANDLE fast reactor, *Annals of Nuclear Energy*, **2009**, 36, 562-566.

61. Okawa T. & Sekimoto H.; A design study on Pb-208 cooled compact CANDLE burning reactor for future nuclear energy supply, *Annals of Nuclear Energy*, **2010**, 37, 1620-1625.
62. Sekimoto H. & Nagata A.; Performance optimization of the CANDLE reactor for nuclear energy sustainability, *Energy Conversion and Management*, **2010**, 51, 1788-1791.
63. Nakae N.; Ozawa T.; Ohta H.; Ogata T.; Sekimoto H.; An approach for evaluating fuel system applied in innovative nuclear energy system, *Progress in Nuclear Energy*, **2011**, 53, 1039-1044.
64. Okawa T. & Sekimoto H.; Design study on Pb-208 cooled CANDLE burning reactors toward practical application for future nuclear energy source, *Progress in Nuclear Energy*, **2011**, 53, 886-890.
65. Nakayama S.; Okawa T.; Sekimoto H.; Power control of CANDLE reactor by coolant flow rate, *Progress in Nuclear Energy*, **2011**, 53, 891-894.
66. Okawa T.; Nakayama S.; Sekimoto H.; Design study on power flattening to sodium cooled large-scale CANDLE burning core with using thorium fuel, *Energy Conversion and Management*, **2012**, 53, 182-188.
67. Su'ud Z. & Sekimoto H.; The prospect of gas cooled fast reactors for long life reactors with natural uranium as fuel cycle input, *Annals of Nuclear Energy*, **2013**, 54, 58-66.
68. Nakae N.; Ozawa T.; Ohta H.; Ogata T.; Sekimoto H.; An approach for evaluating the integrity of fuel applied in innovative nuclear energy systems, *Journal of Nuclear Materials*, **2014**, 446, 1-9.
69. Sekimoto H. & Nakayama S.; Power level control of CANDLE reactor without control rods, *Annals of Nuclear Energy*, **2014**, 63, 427-431.
70. Zheng M.; Tian W.; Chu X.; Zhang D.; Wu Y.; Qiu S.; Su G.; Study of traveling wave reactor (TWR) and CANDLE strategy: A review work, *Progress in Nuclear Energy*, **2014**, 71, 195-205.
71. Ellis T. et al.; Traveling-wave reactors : A truly sustainable and full-scale resource for global energy needs, *In : Proceedings of ICAPP'10*, **2010**, 10189.
72. Ahlfeld C. et al.; Conceptual design of a 500 MWe traveling wave demonstration reactor plant, *In : Proceedings of ICAPP'11*, **2011**, 11199.
73. Zhang D.; Chen X.N.; Flad M.; Rineiski A.; Maschek W.; Theoretical and numerical studies of TWR based on ESFR core design, *Energy Conversion and Management*, **2013**, 72, 12-18.
74. Hejzlar P. et al.; Terrapower, LLC traveling wave reactor development program overview, *Nuclear Engineering and Technology*, **2013**, 45, 731-744.
75. Smith C.F.; Halsey W.G.; Brown N.W.; Sienicki J.J.; Moisseytsev A.; Wade D.C.; SSTAR: The US lead-cooled fast reactor (LFR), *Journal of Nuclear Materials*, **2008**, 376, 255-259.
76. Colombo M.; Cammi A.; Memoli V.; Papini D.; Ricotti M.E.; Transfer function modeling of the lead-cooled fast reactor (LFR) dynamics, *Progress in Nuclear Energy*, **2010**, 52, 715-729.

77. Cinotti L.; Smith C.F.; Sekimoto H.; Mansani L.; Reale M.; Sienicki J.J.; Lead-cooled system design and challenges in the frame of Generation IV international forum, *Journal of Nuclear Materials*, **2011**, 415, 245-253.
78. Alemberti A.; Smirnov V.; Smith C.F.; Takahashi M.; Overview of lead-cooled fast reactor activities, *Progress in Nuclear Energy*, **2014**, 77, 300-307.
79. Locatelli G.; Mancini M.; Todeschini N.; Generation IV nuclear reactors: Current status and future prospects, *Energy Policy*, **2013**, 61, 1503-1520.
80. Ueda N.; Kinoshita I.; Minato A.; Kasai S.; Yokoyama T.; Maruyama S.; Sodium cooled small fast long-life reactor "4S", *Progress in Nuclear Energy*, **2005**, 47, 222-230.
81. Horie H.; Miyagi K.; Nakahara K.; Matsumiya H.; Safety performance of the 4S reactor on the ATWS events – statistical estimation of uncertainty, *Progress in Nuclear Energy*, **2008**, 50, 179-184.
82. Ishii K.; Matsumiya H.; Handa N.; Activities for 4S USNRC licensing, *Progress in Nuclear Energy*, **2011**, 53, 831-834.
83. Koreshi Z.U. & Hussain S.Z.; A neutronic pin cell and full-core design analysis of the 4S reactor, *Annals of Nuclear Energy*, **2014**, 72, 145-150.
84. Choi S.Y.; cho J.H.; Bae M.H.; Lim J.; Puspitarini D.; Jeun J.H.; Joo H.G.; Hwang I.S.; PASCAR: Long burning small modular reactor based on natural circulation, *Nuclear Engineering and Desgin*, **2011**, 241, 1486-1499.
85. Salvatores M.; Khalil H.; Bignan G.; Hill R.; Jacqmin R.; Tommasi J.; Advanced fast reactor development requirements: Is there any need for HEU?, *Nuclear Engineering and Design*, 2007, 237, 814-822.
86. Kim T.K.; Grandy C.; Hill R.N.; A 100MWe advanced sodium-cooled fast reactor core concept, *In: PHYSOR 2012*, **2012**.
87. Kim Y.S.; Hofman G.L.; Yacout A.M.; Kim T.K.; U-Mo alloy fuel for TRU-burning advanced fast reactors, *Journal of Nuclear Materials*, **2013**, 441, 520-524.
88. Tak T.W..; Lee D.J.; Kim T.K.; Design of ultralong-cycle fast reactor employing breed-and-burn strategy, *Nuclear Technology*, **2013**, 183, 427-435.
89. Tak T.W.; Lee D.J.; Kim T.K.; Hong S.G.; Optimization study of ultra-long cycle fast reactor core concept, *Annals of Nuclear Energy*, **2014**, 73, 145-161.
90. Eoh J.H.; Lee T.H.; Lee K.L.; Lee H.Y.; Hwang I.G.; Lee Y.B.; Test requirements for the integral effect test to simulate a sodium-cooled fast reactor, *Korea Atomic Energy Research Institute*, KAERI/TR-4424/2011, **2011**.
91. Han S.; Kim J.H.; Bang I.C.; Subchannel analysis of a small ultra-long cycle fast reactor core, *Nuclear Engineering and Design*, **2014**, 270, 389-395.

92. Ha K.S.; Jeong H.Y.; Comparison of the decay heat removal systems in the KALIMER-600 and DSFR, *Nuclear Engineering and Technology*, **2012**, 44, 535-542.
93. Hahn D.H.; Kim Y.I.; Lee C.B.; Kim S.O.; Lee J.H.; Lee Y.B.; Kim B.H.; Jeong H.Y.; Conceptual design of the sodium-cooled fast reactor KALIMER-600, *Nuclear Engineering and Technology*, **2007**, 39, 193-206.
94. Park J.P.; Jeong J.H.; Lee T.H.; Scientific design of a large-scale sodium thermal-hydraulic test facility for KALIMER-Part II: Validation of reactor pool design using CFD analyses. *Annals of Nuclear Energy*, **2015**, 76, 439-450.
95. Kang S.R.; Ha K.S.; Kim H.T.; Kim J.H.; Bang I.C.; An experimental study on natural convection heat transfer of liquid gallium in a rectangular loop, *International Journal of Heat and Mass Transfer*, **2013**, 66, 192-199.

Acknowledgement

2009 년 9 월에 UNIST 에 입학하여 2015 년 6 월에 학위 논문을 마지막으로 모든 과정을 마치고 이렇게 감사의 글을 씁니다.
감사의 글을 쓰는 순간이 온다면 쓰고 싶은 말이 많았으나 정작 이 시간이 되고 보니 지도 교수님과 랩원 들의 얼굴만 떠오르네요.

6 년 동안 지도해주시고 훈련시켜주신 방인철 교수님.
교수님을 보면서 좋아하는 일을 하시는 분의 삶이 얼마나 행복한 지에 대해 깨달을 수 있었습니다. 교수님의 가르침을 100% 제 것으로 만들었다라고 자신 있게 말할 수는 없지만 지금까지 해주셨던 조언들은 항상 마음 깊이 새기고 살겠습니다. 뼈 속 깊이 감사 드립니다.

더불어, 바쁘신 가운데 논문 심사를 해주셨던 김지현 교수님, 박형욱 교수님, 이재영 교수님, 최기용 박사님께도 이 자리를 빌어 감사 드립니다

열수력 랩의 초기 랩장이자 대전에 계시는 이승원 박사님.
오빠를 통해 많은 것을 배웠고 또 함께 랩 생활을 하던 그 때가 그립네요. 대전에 가셨어도 가끔 도움이 필요하면 즉각 도와주셨던 모습이 떠올라 감사의 말을 전합니다. 재준이와 언니도 보고 싶네요.

저의 유일한 동기이지만 인생 선배이신 박성대 박사님

아마 제일 많이 싸웠고 제일 많이 화해하고 제일 많은 추억을 공유한 사이가 아닌가 싶네요. 제가 가지지 못한 부분을 가지고 계셔서 배우려고 나름 노력했으나 아직 멀고 먼 길입니다.

대학원 동기는 아니지만 제 친구인 김성만

널 보면 성경에 나오는 온유한 사람의 대표적인 표본이 아닌가 항상 생각해. 내 뾰족한 성격을 널 보면서 고치려고 노력했으나 항상 실패하네. 가까운 곳에 있으니 조만간 만나러 갈께.

막내 같지 않은 막내였으나 지금은 맏이가 된 서한

너의 석사 때 모습은 생각이 나지 않지만 점점 발전해가는 너를 보면서 참 부럽다는 생각을 많이 했어. 예전에는 형들과 누나 사이에서 지금은 동생들 사이에서 너가 맡은 일들을 해나가는 것을 보면서 대단하다는 생각을 한다. 항상 파이팅이야

항상 밤새는 목이 쉰 김경모

너의 첫인상은 별로였으나 지금은 최고인듯.

해결되지 않은 문제에 잠을 포기하면서 수행하는 그 열정에 찬사를 보낸다. 이건 진심임. 내 투덜거림도 잘 받아주고 먼저 말 걸어주고 그래서 항상 고마웠어 건강 잘 챙기고 끝까지 열정적으로 달리길 바래.

건강식품 잘 챙겨먹는 서석빈

너 덕분에 귤에 선식에 떡에 많이 얻어먹었어.

해결되지 않은 문제에 대해 같이 토론해 주고 먼저 물어봐 준 기억이 가장 많이 나는 듯. 너의 그 현명함에 많은 도움을 받아 감사하게 생각해. 밥 잘 챙겨먹고 실험 마무리 잘 되길 기원해.

물건을 안 버리는 문성보

내 잔소리 다 받아주고 불평하지 않고 그대로 따라주는 모습에 신기하다는 생각을 많이 했지. 자리가 근처에 없을 때보다 지금이 더 친해진 듯한 느낌은 들지만 서먹서먹해도 언제나 선배 대접해줘서 고마웠어. 번득이는 아이디어로 학위 과정 잘 마치길 바랄게.

책상 정리가 필요한 김인국

예전엔 건희 친구였지만 지금은 아님.

자연순환 실험 장치도 물성치 생성 파일도 모두 너가 하게 되었네. 좀 더 잘해서 주었으면 좋았을 후회가 항상 남아 미안한 마음이 들어. 같이 프로그래밍 학원도 다니면서 신세도 많이 졌고 덕분에 고마웠어. 지금 하는 실험, 제작하는 장치 모두 마무리 잘하고 좋은 논문 쓰길 바래.

긴 머리를 잘 관리하는 정영신

코드 함께 할 때부터 잘한다는 생각은 했었지만 대학원 올라와서 포텐을 터트려준 후배. 널 통해 나는 박사 과정 마지막에 정말 많은 걸 배웠어. 유경이와 함께 랩의 여자사람으로서 청결과 잔소리를 부탁한다. 넌 어디서든 뭘 하든 잘할 듯.

무슨 생각하는지 잘 모르겠는 허효

많은 말을 나누진 못했지만 자료는 많이 나눈 듯. 고속로 과제를 시작하면서 나도 그 덕분에 많이 배운 것 같아. 항상 지금처럼 열심히 살길 바라고 이젠 아니겠지만 또 필요한 자료있음 연락해.

화 한번 안내는 신유경

널 보면서 어떻게 항상 웃을 수 있을까 라는 생각을 많이 했어. 코드 공부 같이 하면서 참 착하다는 생각을 많이 했지. 밥 사준다는 약속 꼭 지키고 필요한 일 있으면 미리 연락하길 부탁한다.

냉매가 생각나는 손규민

냉매 물성치를 마무리 하지 못하게 되어 미안해. 신경 많이 써주지 못한 점이 마음에 좀 걸리기도 하고, 내가 공부할 때보다 더 깊이 생각하는 점에 놀랍기도 했어. 언젠가 시뮬레이션을 성공 시키면 나에게도 꼭 연락해주길.

우리 랩은 아니지만, 항상 힘이 되어준 동한오빠, 석사 때 친하게 지낸 정석오빠, 지금은 외국에 나가 있는 종진오빠, 가끔씩 연락도 하고 얼굴도 보는 병진오빠, 최근에 얼굴 본 주앙오빠, 다시 직장으로 돌아간 내 친구 이경주, 이야기 잘 들어주는 최경준, 내 밥친구이자 개그 코드가 맞는 최상일, 내 배프였으나 지금은 저 멀리 있는 이주영, 김지현, 최현정, 대학교 후배이자 믿음의 친구인 탁태우, 항상 웃으며 인사하던 최지원, 믿음의 친구 이수민. 모두모두 고마워요.

실험 장치 제작에 도움을 주셨던 대원전열 박영전 부장님, 델타전열 신성영 사장님. 동아계기 민덕기 이사님. 항상 귀찮게 해드려도 잘 설명해 주시고 같이 고생해 주셔서 정말 감사 드립니다.

항상 절 위해 기도해주셨던 반석교회 목사님, 사모님, 내 친구 김요한, 웃으며 반겨주던 김정민, 그 부지런함에 항상 놀라는 민호오빠와 은경언니, 놀라운 개그력을 보여주신 나영언니, 제 잔소리도 받아주던 인현오빠, 재수오빠, 이제서야 친해진 혜정언니 모두모두 아쉽고 감사드립니다.

또한 제 인생에 멘토가 되셨던 지금은 은퇴하신 김영인 교수님. 이 글을 보실 날이 언젠가 오기를 손꼽아 기다립니다. 지금은 미국에 그리고 서울에 있는 남희와 소연이. 항상 잊지 않고 연락해주고 나의 하소연도 들어줘서 고마워 곧 만나러 갈께.

대학원 과정뿐만 아니라 태어나면서부터 지금까지 절 위해 물심양면으로 기도로 지원사격해주신 강승대 목사님과 최순옥 사모님. 엄마, 아빠 고맙고 사랑해요. 그리고 내 동생들 한나, 안나. 고맙다는 말로는 설명이 안될 정도로 모두 고맙고 사랑합니다.
오래오래 사셔서 우리 세 딸과 함께 성지순례 꼭 같이 가요. 이제 곧 만나러 갑니다.

태어나기 전부터 저를 택하시고 지금도 지켜보고 계시는 하나님. 소중한 인연도 과정도 불평하던 순간까지도 모두 감사 드립니다. 앞으로도 좋은 친구가 되어 주시길 바랍니다.